ACS NANO

www.acsnano.org

ARTICLE

Mucus Penetration of Surface-Engineered Nanoparticles in Various pH Microenvironments

Yiyang Guo, Yubin Ma, Xin Chen, Min Li, Xuehu Ma, Gang Cheng, Changying Xue, Yi Y. Zuo, and Bingbing Sun*

Cite This: *ACS Nano* 2023, 17, 2813−2828

Read Online

ACCESS | Metrics & More | Article Recommendations | Supporting Information

ABSTRACT: The penetration behavior of nanoparticles in mucous depends on physicochemical properties of the nanoparticles and the mucus microenvironment, due to particle−mucin interactions and the presence of the mucin mesh space filtration effect. To date, it is still unclear how the surface properties of nanoparticles influence their mucus penetration behaviors in various physiological and pathophysiological conditions. In this study, we have prepared a comprehensive library of amine-, carboxyl-, and PEG-modified silica nanoparticles (SNPs) with controlled surface ligand densities. Using multiple particle tracking, we have studied the mechanism responsible for the mucus penetration behaviors of these SNPs. It was found that PEG- and amine-modified SNPs exhibited pH-independent immobilization under iso-density conditions, while carboxyl-modified SNPs exhibited enhanced movement only in weakly alkaline mucus. Biophysical characterizations demonstrated that amine- and carboxyl-modified SNPs were trapped in mucus due to electrostatic interactions and hydrogen bonding with mucin. In contrast, high-density PEGylated surface formed a brush conformation that shields particle−mucin interactions. We have further investigated the surface property-dependent mucus penetration behavior using a murine airway distribution model. This study provides insights for designing efficient transmucosal nanocarriers for prevention and treatment of pulmonary diseases.

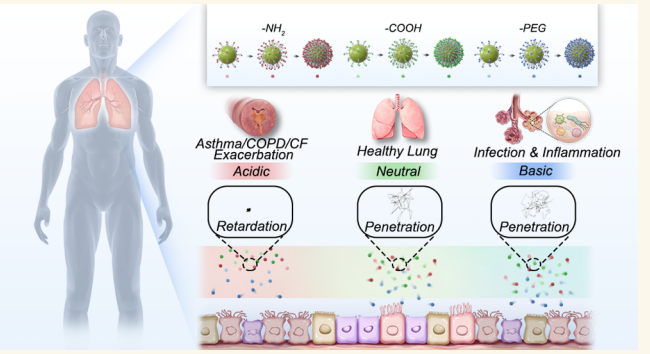

KEYWORDS: *mucus penetration, mucus pH microenvironment, surface engineering, multiple particle tracking, silica nanoparticle*

Inhaled medications delivered by nano- or microsized carriers are widely used for the prevention and treatment of lung diseases such as cystic fibrosis (CF),[1] chronic obstructive pulmonary disease (COPD),[2] asthma,[3] and COVID-19.[4,5] During the transport of the drug carriers in the airway, mucus lines the surface of the airway and hinders the effective delivery of active ingredients.[6,7] The mucus layer is composed of 98% water, 1.6% mucin, and 0.4% of the remainder, e.g., cellular debris, salts, DNA, lipids, and globular proteins.[8] Mucin forms a three-dimensional network to restrain the movement of particles *via* the size exclusion and interaction filtration effect.[9,10] It has been demonstrated that proper control of physicochemical properties of carriers could improve the transport and fate of medications.[11,12]

The neutral charge and hydrophilic surface have been identified as critical requirements for effective trans-mucus drug carriers.[13] Poly(ethylene glycol) (PEG) has been used as an stealth polymer that repels protein adsorption to assist the drug carriers in escaping the binding of mucin.[14,15] Their molecular weight,[16] chain length,[17] and content[18] have been shown to affect mucus penetration performance. The zwitterionic design[19−21] mimics the surface characteristics of the virus surface and further exhibits the equal densities of positive and negative charges without the presence of hydrophobic patches.[22] The surface modification by a zwitterionic polymer[23,24] and density adjustment enable enhanced mucus penetration of particles.[22] Furthermore, the particle surface modifications by block copolymer (F-127),[25] peptides,[26] and protein[27] were potentially alternative strategies to improve the penetration ability of particles. Although PEGylation is often considered as a

Received: November 8, 2022
Accepted: January 27, 2023
Published: January 31, 2023

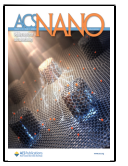

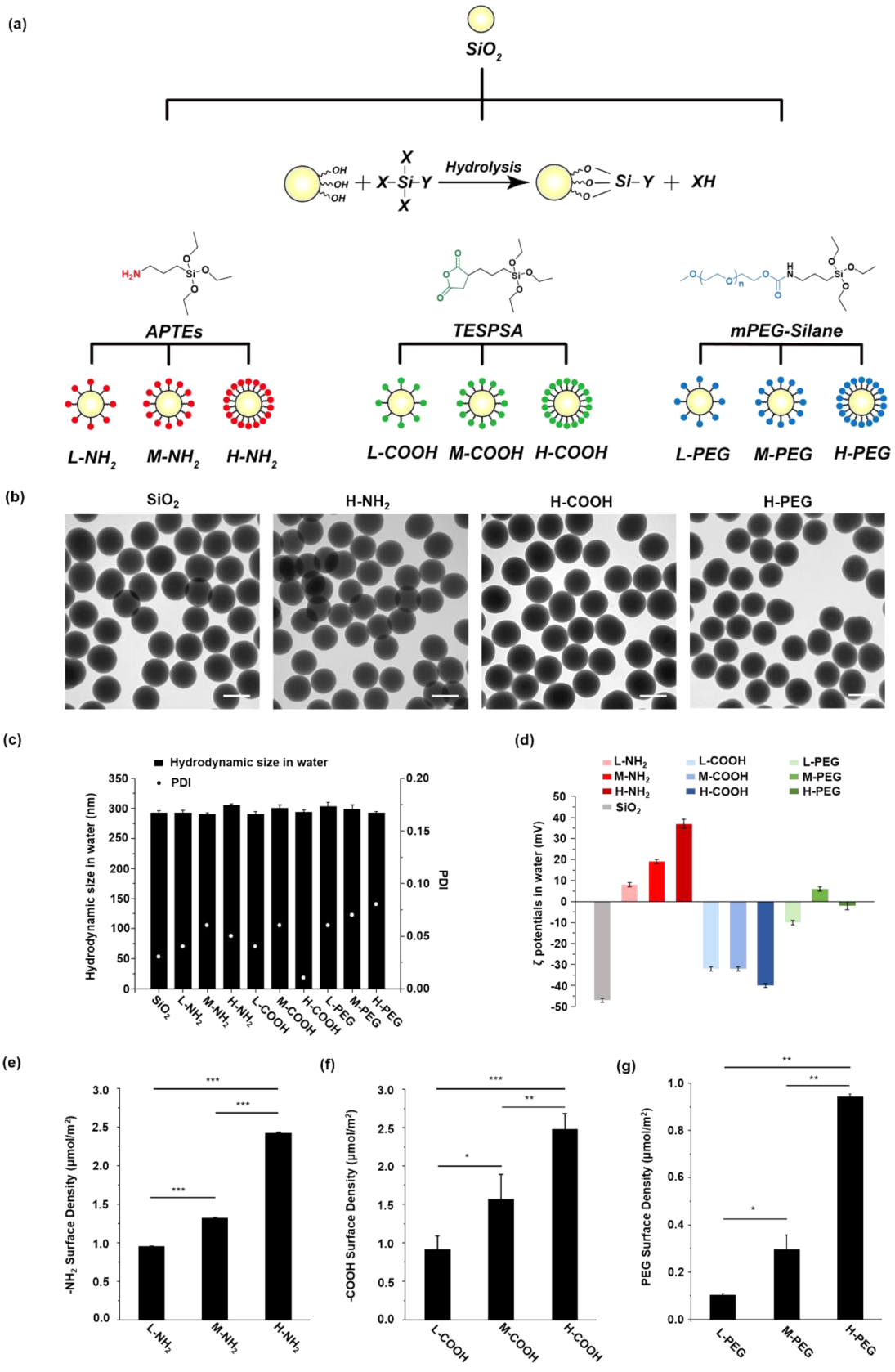

Figure 1. Preparation and characterization of engineered silica nanoparticles with controlled surface modification. (a) Scheme showing the silica nanoparticle synthesis routes. (b) TEM image of pristine and surface-modified silica nanoparticles. The scale bar is 300 nm. (C) The hydrodynamic sizes, PDI, and (d) zeta potentials of silica nanoparticles in water. Quantitative analysis of (e) amine, (f) carboxyl, and (g) PEG densities on silica nanoparticles. *$p < 0.05$, **$p < 0.01$, and ***$p < 0.001$.

https://doi.org/10.1021/acsnano.2c11147
ACS Nano 2023, 17, 2813−2828

"gold standard" to assess mucus penetration, and various surface modification strategies have been proposed, the mechanistic understandings of particle surface property-mediated mucus penetration are currently missing.

The mucus microenvironment changes according to the physiological and pathological states.[28−30] In asthma-exacerbated (pH = 5.2 ± 0.2),[31] healthy (pH = 7.1 ± 0.1),[30] and airway infection or inflammation (pH = 7.2−8.3) states,[32] the pH values of mucus vary. The different pH values affect the microstructure and rheological properties of the mucus[33,34] and change the surface characteristics of NPs.[35] However, the impact of mucus pH microenvironments on the fate of nanoparticles during mucus penetration is rarely considered.

In this study, a comprehensive library of surface-engineered silica nanoparticles (SNPs) was prepared to study their movement in mucus with various pH values mimicking different physiological and pathological environments. Furthermore, the factors affecting the fate of particles in the mucus were elucidated at the molecular level from three aspects, i.e., mucus properties, particle surface properties, and particle−mucin interaction. It is noteworthy that the fate of particles in mucus was dependent on mucus pH, surface ligand type, and density. An acidic mucus environment inhibits the diffusional movement of particles, and the modulation of particle surface ligand density can alter the fate of particles in mucus after functional group modification. This study provides an engineered approach to control the mucus-penetrating capabilities of a drug delivery carrier for the personalized treatment and prevention of pulmonary diseases.

RESULTS

Synthesis and Characterization of Engineered Silica Nanoparticles with Controlled Surface Modification. According to the size exclusion mechanism of mucus, nanoparticles with a size range of 200−500 nm in diameter can more easily penetrate the mucus barrier.[36] Therefore, 300 nm SNPs were selected to study their mucus penetration ability. The pristine SNPs were synthesized using the Stöber method,[37,38] and SNPs were doped with fluorescein isothiocyanate (FITC) for particle tracking (Table S1). Then, SNPs were further modified with silane coupling agents to prepare a library of engineered SNPs with controlled functional groups and ligand densities (Figure 1(a)). Transmission electron microscopy (TEM) analysis showed that SNPs were all spherically shaped and exhibited a uniform morphology and distribution. Surface modification did not affect their primary sizes, and they remained at 300 nm in diameter (Figure 1(b)). The hydrodynamic sizes of pristine and modified SNPs in water were all around 300 nm with polydispersity indexes (PDIs) less than 0.1 (Figure 1(c)). The surface functionalization of SNPs was demonstrated by the change of their zeta potentials. Compared to pristine SNPs, their zeta potentials became positive after amine modification and were positively correlated with amine density. After carboxyl modification, their zeta potentials were around −35 mV in water, and it was not density-dependent. For the PEG-modified SNPs, their zeta potentials were close to neutral (Figure 1(d)).[39] Furthermore, the densities of functional groups were quantitatively determined.[38] The low-, middle-, and high-density amine was 0.95, 1.32, and 2.42 μmol/m^2, respectively (Figure 1(e)). The low-, middle-, and high-density carboxyl was 0.91, 1.57, and 2.48 μmol/m^2, respectively (Figure 1(f)). For PEG modification, the low-, middle-, and high-density was 0.11, 0.30, and 0.94 μmol/m^2, respectively (Figure 1(g)). The relatively lower PEG density may be caused by higher steric hindrance.[40,41]

Mucus-Penetrating Ability of Engineered Silica Nanoparticles in Artificial Mucus with Different pH Values. The pH value of healthy lung airway mucosal surfaces is closed to neutral,[32] while in a diseased state, the pH regulatory mechanism is compromised, and the pH of the mucus shifts to an acidic or alkaline environment,[42−44] which could affect the delivery of nanosized carriers. Thus, alginic (Alg) hydrogels and commercial mucin were formulated in artificial mucus to restore the physical and chemical properties of native mucus.[45,46] By proper selection of Ca^{2+} concentration (2 mg/mL), the artificial mucus was able to reproduce the steric and interactive barrier of native mucus (Figure S1 and Table S2). The pH values were adjusted to mimic the mucus with different states,[30] and multiple particle tracking (MPT) was used to evaluate the motility behavior of particles in mucus. Due to the isotropic nature of mucus composition, the motion of SNPs in two dimensions (2D) was used to resemble the one in three dimensions (3D).[47]

When the high-density amine- and carboxyl-modified SNPs were dispersed in acidic mucus, larger agglomerations were observed, and particles were trapped in mucus. In contrast, SNPs with higher PEG density diffused more freely (Videos S1−S3). The aggregation and agglomeration between particles due to pH change were excluded by sonication[48] and zeta potential analysis, respectively. Thus, the NP−mucin interaction was a predominant factor that led to the aggregation of particles. When the pH environment of mucus was shifted to neutral (pH = 7.0) or slightly alkaline (pH = 7.7) ones, the aggregation of particles disappeared, and the diffusion of SNPs was significantly improved, with the appearance of monodisperse motion (Videos S1−S3). The ensemble mean squared displacement (⟨MSD⟩) was used to evaluate the time-dependent displacement of SNPs, which was positively correlated with their mucus penetration ability.[47,49] When SNPs with high-density amine and carboxyl were in mucus of pH = 7.0 and pH = 7.7, their ⟨MSDs⟩ were increased by 2 orders of magnitude compared to those in acidic mucus. For high-density PEG modification, the pH-mediated changes in ⟨MSD⟩ were not significant (Figure 2(a−d)). Furthermore, the logarithms of the effective diffusion coefficient (D_{eff}) were calculated. For SNPs with amine, carboxyl, and PEG, the D_{eff} values in the mucus at pH = 7.0 and 7.7 were about 30 times higher than those in the acidic mucus (Figure 2(e−g)), further confirming the improved diffusion ability of SNPs with surface modification in neutral and weak alkaline environments.

The anomalous exponent (α) represents the heterogeneity of mucus properties and the difference of restriction for nanoparticles in the mucus.[47] The cutoff value of α for the trajectory of each SNPs was set to 0.5 to classify the SNPs as trapped (α < 0.5) or diffusive (α > 0.5).[50,51] According to this criterion, 92.3%, 88.2%, and 52.2% of SNPs with high-density amine, carboxyl, and PEG were trapped in acidic mucus (pH = 5.2), respectively (Figure 2(h)). In the neutral mucus, this percentage was dropped to 21.6%, 37.3%, and 34.8%, respectively (Figure 2(i)). In the mucus with pH = 7.7, the percentages were 15.4%, 29.7%, and 33.5%, respectively (Figure 2(j)). It indicated that, with the increase of pH, the movement of SNPs with surface-controlled modification in mucus gradually changes from a state of retention to diffusion. The consistent trends of ⟨MSD⟩, D_{eff}, and α were also found in the low- and middle-density modified SNPs with amine, carboxyl, and PEG (Figure 2). Similarly, pristine SiO_2 also showed pH-dependent mucus movement.

https://doi.org/10.1021/acsnano.2c11147
ACS Nano 2023, 17, 2813−2828

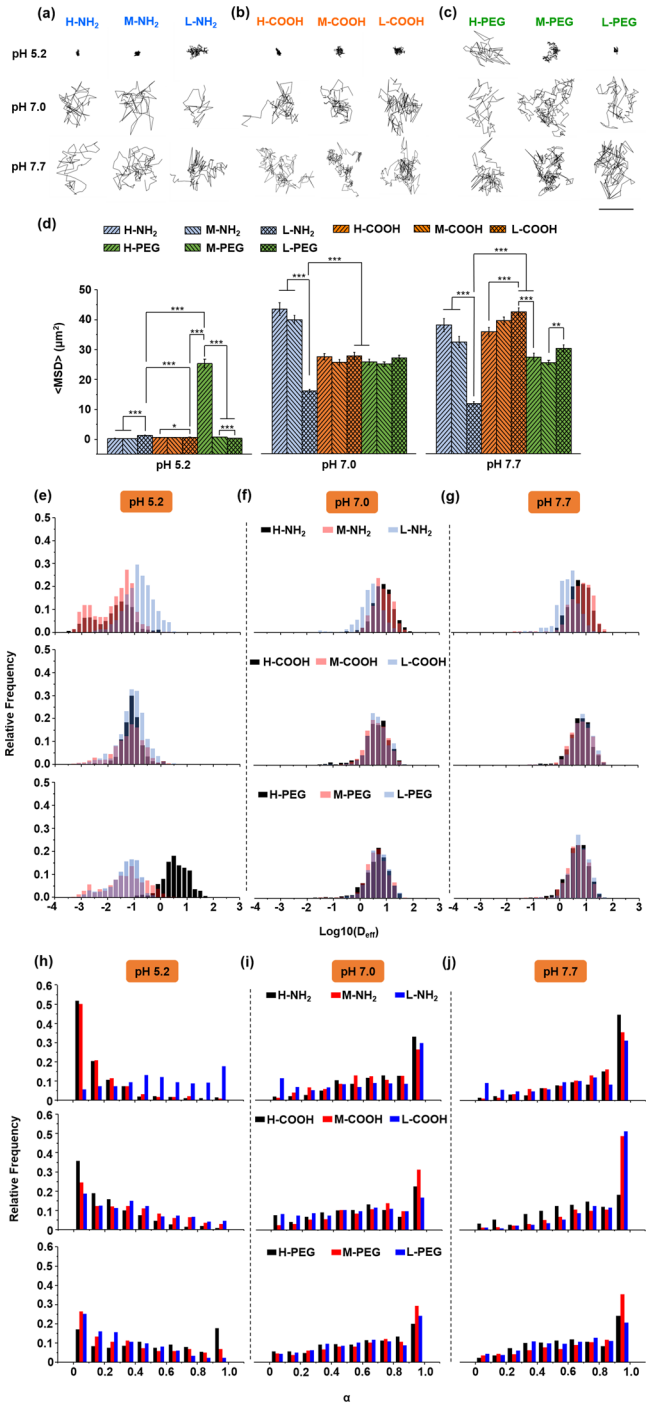

Figure 2. Determination of mucus-penetrating ability of surface-modified silica nanoparticles in artificial mucus using MPT. (a−c) Representative trajectories and (d) ensemble mean squared displacement of silica nanoparticles with different modification densities in acidic (pH 5.2), neutral (pH 7.0), and alkaline (pH 7.7) artificial mucus. The scale bar is 500 nm. Data represent means ± SEM, *$p < 0.05$, **$p < 0.01$, and ***$p < 0.001$. The distribution of the logarithms of effective diffusivities (D_{eff}) for silica nanoparticles that modified amine, carboxyl, and PEG groups with different densities in (e) acidic (pH 5.2), (f) neutral (pH 7.0), and (g) alkaline (pH 7.7) artificial mucus. The anomalous exponent of silica nanoparticles that modified amine, carboxyl, and PEG groups with different densities in (h) acidic (pH 5.2), (i) neutral (pH 7.0), and (j) alkaline (pH 7.7) artificial mucus. The time scale is 1 s.

The MSD of particles in mucus with pH 7.7 was similar to that in mucus with pH 7.0, but was 130 times higher than that in mucus with pH 5.2. Additionally, the diffusion coefficient and anomalous exponent were consistent with the trend of MSD (Figure S2).

The types of surface ligand could affect the fate of the particles in the mucus.[48,52,53] Thus, SNPs with similar amounts of amine, carboxyl, and PEG, i.e., 0.95 ± 0.01, 0.91 ± 0.18, and 0.94 ± 0.01 μmoL/m^2, were selected to examine their trans-mucus behaviors (Figure 1(e−g)). In the acidic mucus, PEGylated SNPs exhibited the advantage of mucus penetration, and the ⟨MSD⟩ of PEG-modified SNPs was 20.8 and 42.7 times higher than that of amine- and carboxyl-SNPs, respectively. In contrast, the ⟨MSD⟩ of carboxyl-modified SNPs (27.80 μm^2) was similar to that of PEG-modified SNPs (25.71 μm^2), and both were higher than amine-modified SNPs (16.08 μm^2) in neutral mucus (Figure 2(d)). In alkaline mucus, the carboxyl-SNPs exhibited slightly improved mucus penetration, and their ⟨MSD⟩ was 1.56 and 3.61 times higher than those of PEG-SNPs and amine-SNPs, respectively (Figure 2(d)). As to the D_{eff} and α, they shared similar trends to that of ⟨MSD⟩ (Figure 2(e−j)). Altogether, these results indicated that PEGylated and amine-SNPs exhibited pH-independent mucus penetration and penetration inhibition. For carboxyl-SNPs, the improved mucus penetration was only observed in weakly alkaline mucus.

The density of surface modification is a critical factor in determining the fate of particles in the mucus.[18] In the acidic mucus, although SNPs with amine modifications were shown to be trapped in the mucus (Figure 2(a)), the low-density amine modification (⟨MSD⟩ = 1.21 μm^2) exhibited a better mucus penetration. For carboxyl-modified SNPs, particles were also trapped in mucus (Figure 2(b)). In contrast, after PEGylation, the mucus penetration ability of the particles was increased significantly in a PEG density-dependent manner (Figure 2(c)), and the ⟨MSD⟩ values of low-, middle-, and high-density PEG modification were 0.33, 0.67, and 25.21 μm^2, respectively (Figure 2(d)). In the neutral and weakly alkaline environments, mucus penetration ability of SNPs with amine modification was positively correlated with modification density. The carboxyl-modified SNPs showed the same penetration ability, which was independent of carboxyl ligand density (Figure 2(d)). Therefore, SNPs with extremely higher density of carboxyl (24.19 μmoL/m^2, HH-carboxyl) were prepared to explore the effect of the density of carboxyl groups on the mucus-penetrating ability (Figure S3). The HH-carboxyl SNPs were still trapped in acidic and neutral mucus but showed improved motion in the weakly alkaline environment (Video S4 and Figures S4 and S5).

To verify the experimental results in artificial mucus, the rat ileal mucus was collected to simulate airway mucus due to their similar rheological properties and pH values (pH = 6.5−7.0).[54] Compared to pristine particles, although amine-SNPs' mucus penetration ability was positively correlated with their densities, they were still trapped in mucus (Video S5 and Figure 3(a)). In contrast, the carboxyl density was negatively correlated with mucus penetration (Figure 3(b,c)), and low-density carboxyl-modified particles exhibited mucus penetration ability. For the PEGylated SNPs, density-dependent mucus penetration was observed. The D_{eff} and α showed consistent trends with ⟨MSD⟩ (Figure 3(d,e)). It should be noted that the native mucus was more restrictive than artificial mucus (Videos S1−S5), which has been suggested be related to the complexity and heterogeneity of native mucus composition.[29]

https://doi.org/10.1021/acsnano.2c11147
ACS Nano 2023, 17, 2813−2828

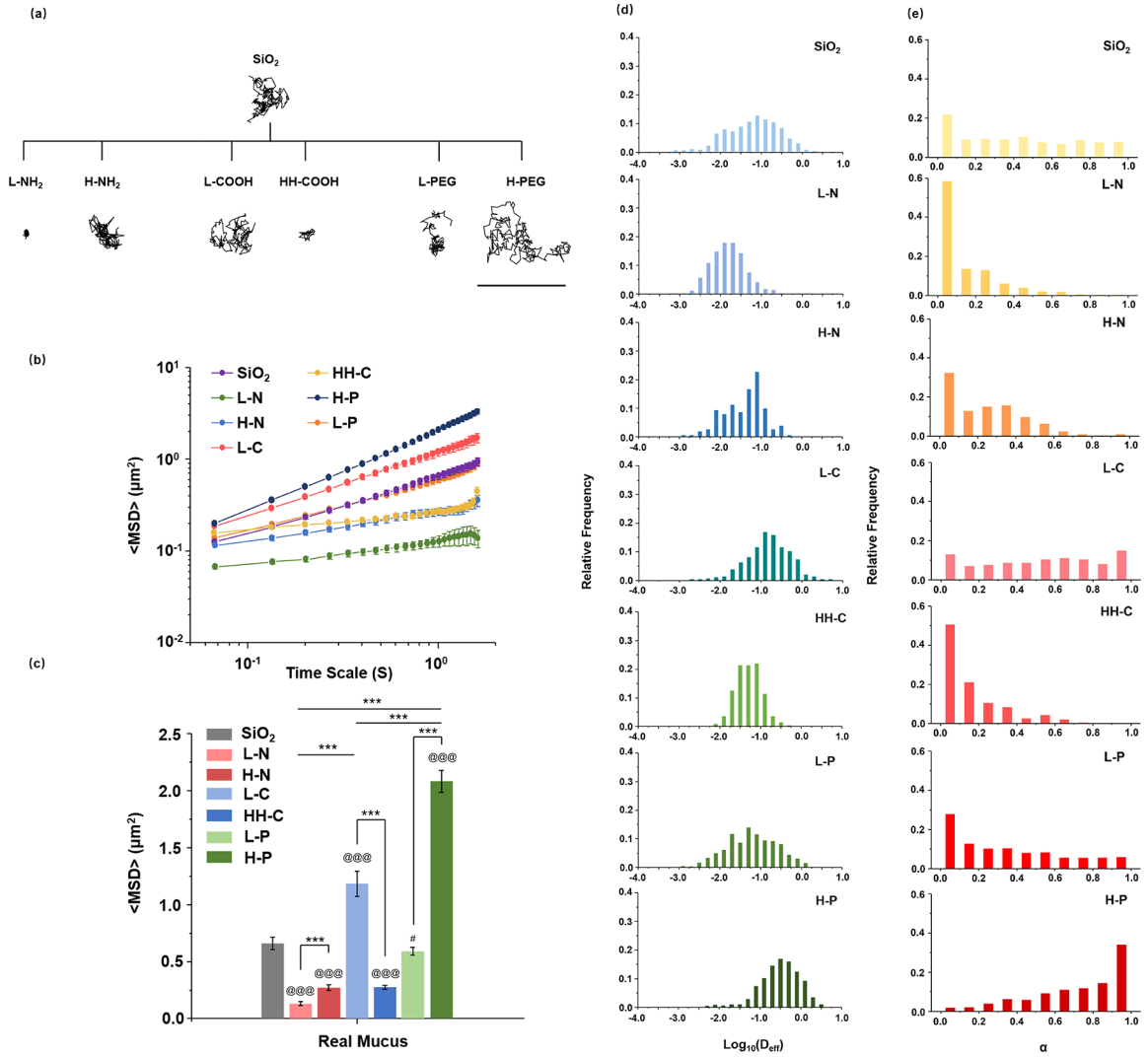

Figure 3. Determination of mucus-penetrating ability of surface-modified silica nanoparticles in rat ileal mucus using the MPT. (a) Representative trajectories of engineered surface silica nanoparticles in rat ileal mucus. The scale bar is 500 nm. (b) Ensemble mean squared displacement of engineered surface silica nanoparticles as functions of the time scale. (c) Ensemble mean squared displacement of engineered surface silica nanoparticles at the time scale of 1 s. Data represent means ± SEM. $^{@@@}p < 0.001$ compared to pristine SNPs; $^{***}p < 0.001$ compared between modified groups. (d) The distribution of the logarithms of effective diffusivities (D_{eff}) and (e) the anomalous exponent (α) of engineered surface silica nanoparticles. The time scale is 1 s.

Mechanistic Analysis of pH-Dependent Mucus Penetration of NPs in Mucus. The mechanism of mucus penetration for surface-controlled SNPs in airway mucus with different pH values was further determined from three aspects, i.e., the mucus macro−micro properties, the surface properties of SNPs, and the interaction between mucus and SNPs (Figure 4(a)).

Mucus pH would affect mucus macro-rheological properties and thus determine the fate of particle movement. Under acidic conditions, the mucus viscosity at lower shear rates plateaued, indicating the ability of mucus microstructure to resist deformation at lower shear rates and a certain cross-linking strength (Figure 4(b)). However, as the shear rate was further increased, the viscosity was decreased and the anti-deformation ability of the mucus was compromised (Figure 4(b)). In contrast, the viscosity decreased linearly with shear rate in the neutral and weakly alkaline mucus, and the cross-linking was too weak to resist shear stress, thus leading to lower mucus microstructure strength (Figure 4(b)). In particular, the viscosity of mucus was further determined at a shear rate of 100 1/s. In the acidic environment, the viscosity was about 5.6 and 7.2 times higher than those at neutral and alkaline pH values, respectively (Figure 4(c)). It confirmed that the mucus cross-link density was negatively correlated with mucus pH. Furthermore, the viscoelastic behavior of artificial mucus under different pH environments was characterized (Figure 4(d)). Independent of pH, the storage modulus (G') was higher than the loss modulus (G''), indicating the gel-like response for mucus. In contrast, the modulus values gradually decreased with the increase of pH, suggesting the degree of mucus cross-linking was negatively correlated with pH values. As mucus cross-linking degree increases, SNPs are more likely to interact with mucins and to be trapped in acidic mucins. In contrast, their movement could be enhanced in neutral and weakly alkaline mucus due to the weakened restriction of Brownian motion in the mucus.

The pH values of the mucus also affect the surface properties of SNPs. In the acidic environment, the positively charged amine-modified SNPs would be trapped in the negatively

https://doi.org/10.1021/acsnano.2c11147
ACS Nano 2023, 17, 2813−2828

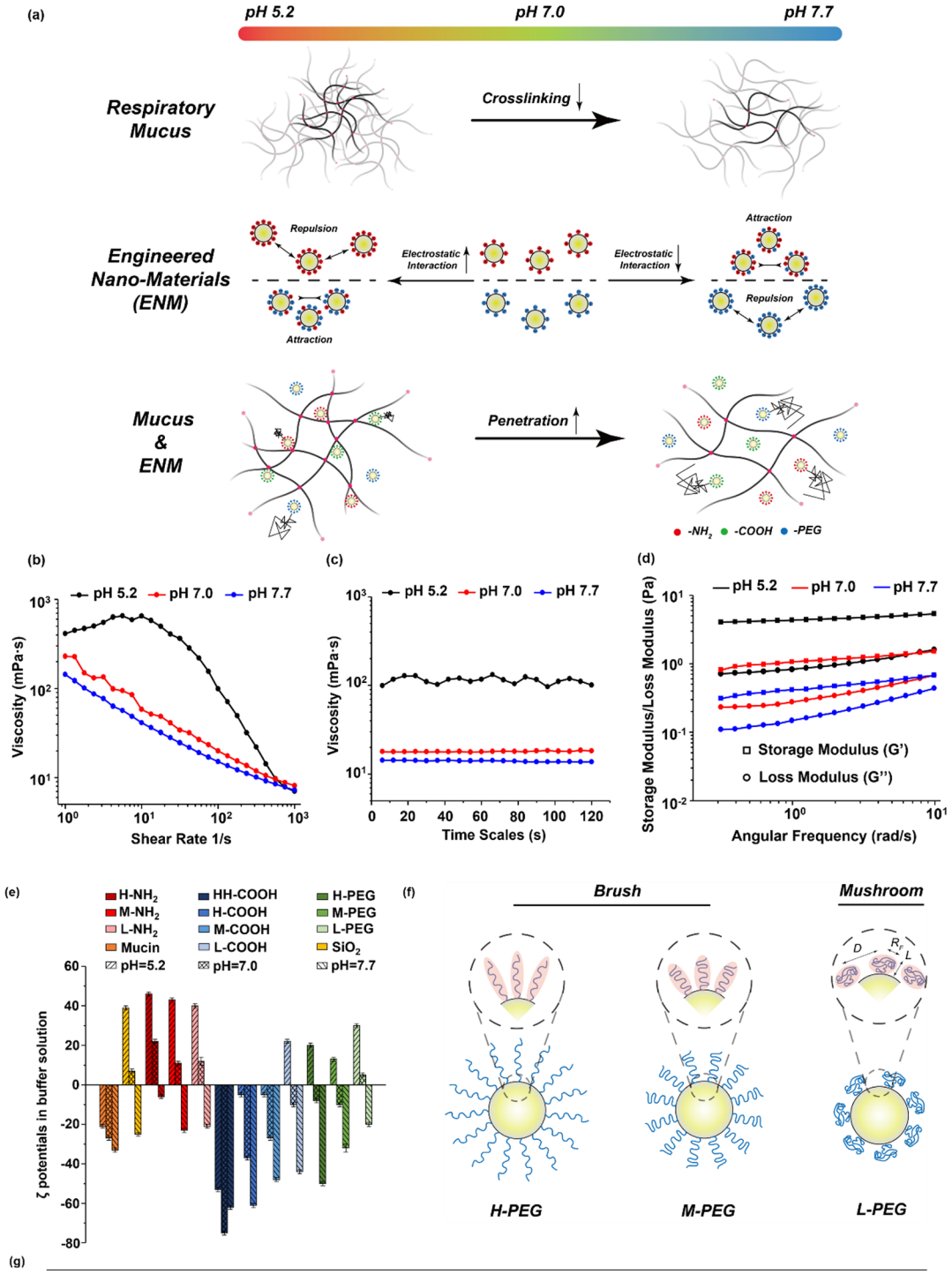

Materials	PEG MW (g/mol)	R_F (nm)	D (nm)	L (nm)	Conformation
H-PEG-SiO_2	2000	3.41	1.50	5.90	Brush (close to dense brush)
M-PEG-SiO_2			2.67	4.01	Brush
L-PEG-SiO_2			4.48	2.84	Mushroom

Figure 4. The mechanistic analysis of mucus penetration of surface-modified silica nanoparticles in artificial mucus with different pH values. (a) Schematic illustration of the mechanism is proposed from the aspects of the mucus system, surface properties of nanoparticles, and the interaction between mucus and silica nanoparticles. (b) The viscosity of artificial mucus at different pH as a function of shear rate in the range of $1-10^3$ s^{-1}. (c) The viscosity of artificial mucus at different pH as a function of time. The shear rate is 100 s^{-1}. (d) The relationship between storage modulus (G')/loss modulus (G''), and angular frequency of artificial mucus at different pH in the frequency range of 0.05−1.6 Hz. All measurements were performed at a strain amplitude of 0.5%. (e) Zeta potentials of mucin and silica nanoparticles in buffer solutions with different pH values. For zeta potential measurement, the mucin and nanoparticles were dialyzed and resuspended in 20 mM NaAc (pH 5.2 and 7.0) and 20 mM MOPS (pH 7.7), respectively. (f) Schematic illustration and (g) conformation analysis of PEG modification on the silica nanoparticle surface.

https://doi.org/10.1021/acsnano.2c11147
ACS Nano 2023, 17, 2813−2828

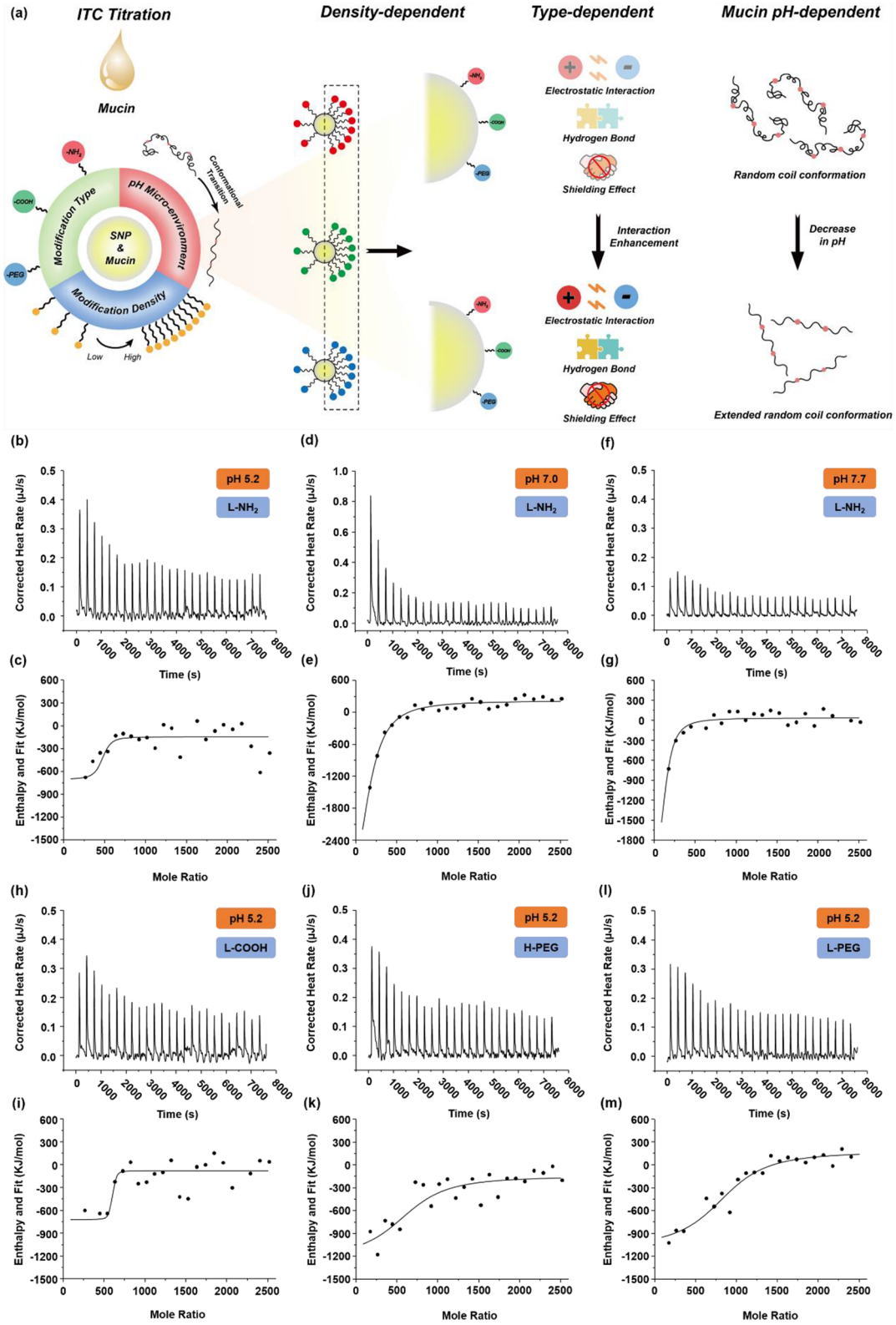

Figure 5. ITC titration and fitted curves of surface-ligand-controlled SNPs and mucin solution with different pH values. 20 mM NaAc (pH 5.2 and 7.0) and 20 mM MOPS (pH 7.7) were used to balance the mucin solution and particle suspension to the same pH value. (a) Schematic illustration of SNP−mucin interaction revealed by using ITC. (b, c) Acidic, (d, e) neutral, and (f, g) alkaline mucin solution titration with low-density amine, (h, i) low-density carboxyl-, (i−k) high-density PEG-, and (l, m) low-density PEG-SNPs. All ITC thermodynamic data were fitted by the NanoAnalyze Data Analysis software, version 3.11.0 (TA Instruments).

charged mucus (Figure 2(a)). In contrast, the amine-modified SNPs exhibited more neutral and negative zeta potential values in both neutral and weakly alkaline environments, respectively (Figure 4(e)). As a result, the electrostatic interaction between amine-modified SNPs and mucin decreased with the increase of environmental pH values. Thus, the mobility of amine-modified

https://doi.org/10.1021/acsnano.2c11147
ACS Nano 2023, 17, 2813−2828

Table 1. Thermodynamic Parameters of the Interaction between SNPs and Mucin

Materials	pH	$K_a/10^8(M^{-1})$	ΔH(kJ/mol)	ΔS(J/mol·K)	ΔG(kJ/mol)	$-T\Delta S$(kJ/mol)
L-PEG	5.2	0.29 ± 0.09	−1045 ± 208	−3363 ± 701	−43 ± 1	1003 ± 209
H-PEG	5.2	0.14 ± 0.03	−1350 ± 283	−4392 ± 950	−41 ± 1	1309 ± 283
L-COOH	5.2	37.6 ± 9.82	−656 ± 19	−2019 ± 65	−55 ± 1	602 ± 19
L-NH_2	5.2	5.63 ± 2.98	−756 ± 166	−2370 ± 557	−50 ± 1	707 ± 166
L-NH_2	7.0	0.26 ± 0.13	−4040 ± 1276	−13410 ± 4283	−42 ± 1	3998 ± 1277
L-NH_2	7.7	0.24 ± 0.15	−3280 ± 1219	−10863 ± 4087	−42 ± 2	3239 ± 1218

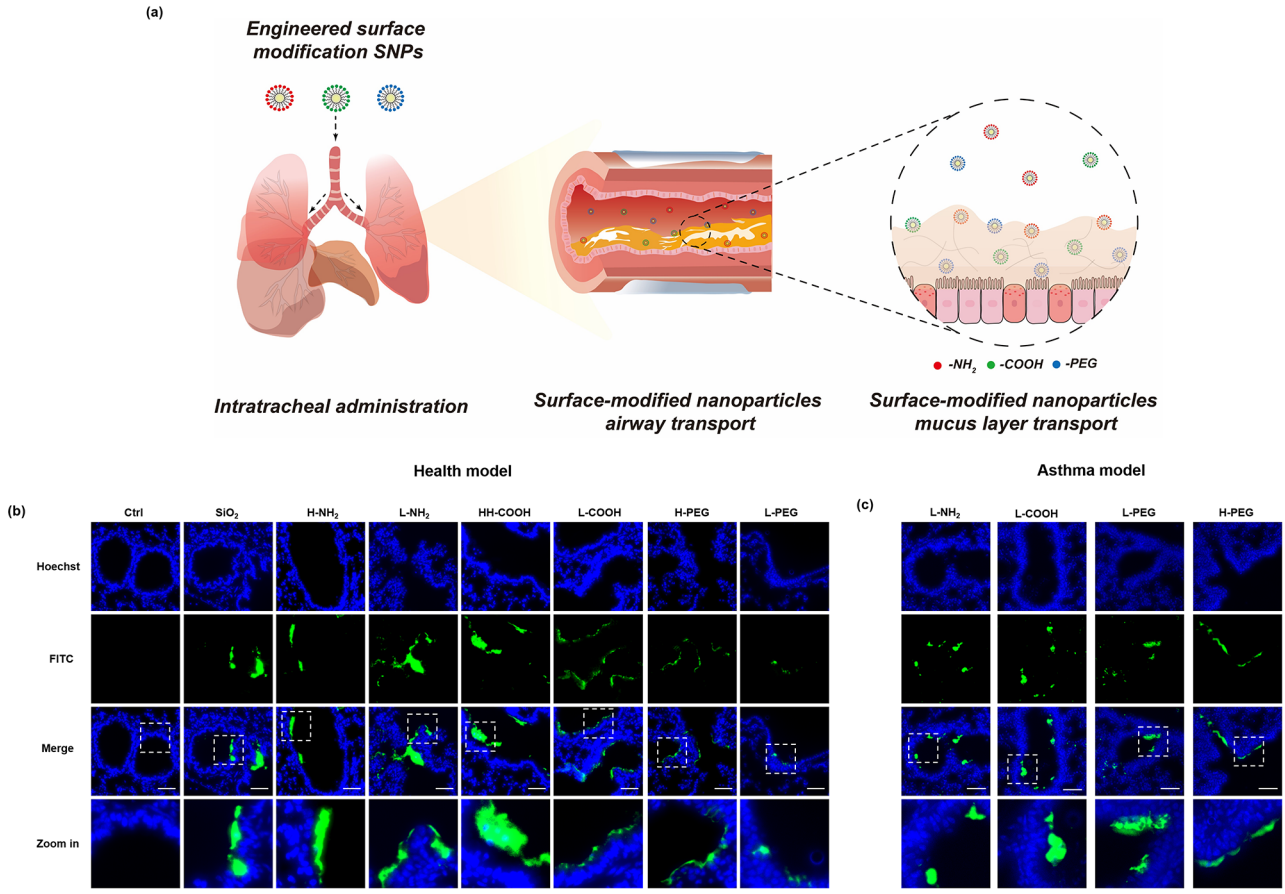

Figure 6. Distribution of silica nanoparticles in the airway of mice. (a). Schematic illustration of the *in vivo* administration method and silica-modified nanoparticle transport in the airway and mucus layer. The distribution of silica-modified nanoparticles in healthy (b) and asthma model (c) murine tracheal at 30 min after administration. The scale bar is 50 μm, n = 3.

SNPs in neutral and weakly alkaline mucus was significantly higher than that in an acidic environment (Figure 2(a)). For the PEGylated SNPs, the zeta potential of low-density particles was 30 ± 1 mV, which was similar to that of pristine SNPs in the acidic condition (pH = 5.2) (Figure 4(e)), indicating that the surface properties of low-density modified PEG were close to pristine SNPs. The zeta potential decreased after modification with middle- and high-density PEG, which was 13 ± 1 and 20 ± 1 mV, respectively. In the neutral and weak alkaline environments, their zeta potentials were shifted to negative values (Figure 4(e)). Thus, the electrostatic interaction between PEG-modified SNPs and mucin was reduced, leading to the enhanced mucus penetration ability (Figure 2). In addition, the surface conformation of PEG (2000 g/mol) modification was determined.[55,56] Low-density PEG modification exhibited a "mushroom" conformation on the surface of SNPs. As a result, more silica core was exposed to mucin. In contrast, the "brush" conformation was obtained with increased PEG density, indicating the PEG shielding layer could isolate the contact between the SNP surface and mucin and enhance the mucus penetration ability (Figure 4(f,g)). Interestingly, for the carboxyl modification, the zeta potential of SNPs was close to neutral at pH = 5.2 (Figure 4(e)). However, their mucus penetration ability was weak (Figure 2). Thus, the remaining noncovalent bonds, such as hydrogen bonding rather than electrostatic interactions, could be the main reason for the interaction between carboxyl-modified SNPs and mucin.[14]

In order to mechanistically understand the effect of mucus pH, ligand type, and density on mucin−particle interactions at the molecular level, representative SNPs were selected and titrated with mucin solution with different pH values by using isothermal titration calorimetry (ITC) (Figure 5). Independent

https://doi.org/10.1021/acsnano.2c11147
ACS Nano 2023, 17, 2813−2828

of the mucus pH and functional groups, the interaction of mucin with SNPs was exothermic and an entropy loss process (Table 1), indicating an enthalpy-driven interaction and the formation of noncovalent bonds, such as hydrogen bond, electrostatic, and van der Waals interactions.[57,58] To study the effect of mucus pH, the amine-modified SNPs were selected to titrate with mucin solutions. The association constant (K_a) of SNPs in an acidic (pH 5.2) environment was an order of magnitude higher than those in neutral (pH 7.0) and slightly alkaline (pH 7.7) ones (Table 1). The stronger SNP−mucin interaction was correlated with particles being trapped in the acidic mucus (Figure 2). In order to examine the effect of ligand type, the SNPs with similar surface ligand density, i.e., amine- (0.95 ± 0.01 μmoL/m^2), carboxyl- (0.91 ± 0.18 μmoL/m^2), and PEG-modified (0.94 ± 0.01 μmoL/m^2) SNPs, were selected to titrate with acidic mucin. The K_a of carboxyl- and amine-SNPs were 2 and 1 order of magnitude higher than that of PEGylated particles, respectively (Table 1), suggesting significantly higher adsorption strength of mucin on carboxyl- and amine-SNPs than that on PEGylated ones. It is worth noting that the K_a of the carboxyl-SNP was 6.7 times higher than that of the amine-SNP (Table 1). Additionally, the K_a of low-density PEGylated SNPs (0.11 μmoL/m^2) was 2.1 times higher than high-density (0.94 μmoL/m^2) PEGylated SNPs (Table 1), which was consistent with our MPT and conformational analyses (Figures 2, 3, and 4).

***In Vivo* Distribution of NPs in Murine Airway.** The surface-mediated mucus penetration was further evaluated by using a murine airway distribution model (Figure 6(a)). The pH value of airway mucus was 6.5−7.0.[59,60] Thirty minutes after administration, the amine- (0.95 ± 0.01 μmoL/m^2), carboxyl- (0.91 ± 0.18 μmoL/m^2), and PEG (0.94 ± 0.01 μmoL/m^2)-modified SNPs were selected to examine the effect of ligand type on mucus penetration. Large amounts of pristine or amine-modified SNPs were accumulated on the surface of the airway. In contrast, PEG- or carboxyl-modified SNPs exhibited uniform and continuous distribution along the transverse sections of the airway (Figure 6(b)). Compared to pristine particles, they could facilitate mucus penetration, exhibited comparable mucus-penetrating ability, and were both stronger than amine-modified SNPs. Notably, the density of surface groups was demonstrated to be a critical factor in determining the fate of materials in mucus. The high-density amine (2.42 μmoL/m^2), HH-density carboxyl (24.19 μmoL/m^2), and low-density PEG (0.11 μmoL/m^2) modified SNPs were administered to the airway. An aggregated and discontinuous distribution was observed (Figure 6(b)). Furthermore, in order to study the effect of this surface-property-dependent mucus penetration behavior in disease state, a mouse asthma model was established. It was shown that the surface-property-dependent mucus penetration behavior was still significant (Figure 6(c)). High-density PEGylated SNPs showed a uniform distribution on the airway surface, while low-density PEG, amine, and carboxyl SNPs aggregate on the airway cross section, which proved that high-density PEG had more advantages in mucus penetration. The airway distribution patterns further suggested that particle fate in mucus was surface ligand type- and density-dependent (Figures 2 and 3).

DISCUSSION

The mucus layer of the airway is not only a line of defense against invasion by foreign pathogens[61−63] but also a barrier to the delivery of active ingredients during inhalation administration.[6] Therefore, the rational design of carriers for mucus penetration plays a critical role in efficient pulmonary drug delivery.[64,65] Herein, we demonstrated that the acidic mucus environment was more restrictive than neutral and weakly alkaline ones because it could enhance mucin−particle interactions by improving the cross-linking properties of mucus and altering particle surface properties. Particles with amine or carboxyl groups exhibited mucoadhesive properties, while PEGylation showed mucus-penetrating properties. Importantly, their motility was a function of surface modification ligand density.

The airway mucus penetration model in the current study is mainly derived from commercial porcine gastric mucin. Regardless of the mucin suspension[66,67] or the artificial mucus,[68,50] the pH value of the system is acidic (pH = 3−5), which is different from the natural airway health neutral mucus environment.[32] Although sputum taken from patients such as with CF[15,69,70] as a surrogate is similar to the mucus environment experienced by drug carriers after airway administration, factors such as the causes (endogenous[71] or exogenous exposure[30]) and states of diseases (mild[72] or severe[31]) were not considered. Acid respiration occurs in exacerbation of CF (mucus pH = 5.3)[73] and asthma (pH = 5.2),[31] but the pH of mucus is increased in mild asthma (pH = 7.6)[72] and stable CF (pH = 5.9).[73] Moreover, the mucus is an alkaline environment (pH = 7.8−8.5)[30] in inflammatory diseases. In this study, the effect of mucus pH on the mucus penetration of carrier particles was investigated. In acidic mucus, the movement of amine- and carboxyl-modified particles was inhibited, while PEG modification facilitated mucus penetration.[52] However, when the pH of mucus was increased, the particle motion was enhanced in general; thus the advantage of PEGylation gradually decreased.[74] A recent study has revealed that mucin undergoes a sol−gel transition in acidic−neutral environments,[75,76] and the cross-linking properties of mucus are stronger in acidic than that in neutral conditions. In our study, it was demonstrated that the pH-dependent changes in mucus macro-rheology and microstructure were the main reasons for the observed variations of particle motion behavior (Figure 2(a−c)).

From the perspective of mucin microstructure, the changes in the macro-crosslink properties of mucus at different pH values were due to the changes in the microstructure of mucin. During the acidification of mucus, carboxylates on mucin were protonated. As a result, the electrostatic interaction between carboxylate and amine groups were compromised, and hydrophobic domains hidden in the salt bridge folded structure were exposed, promoting the cross-linking of mucus gel.[77] This pH-mediated conformational change was also observed in commercially available mucin.[78] In addition to the influence of the hydrophobic domain, electrostatic interactions due to the exposure of mucin glycosyl side chains also play an essential role.[8] In general, mucins are negatively charged due to the sialic and sulfate components in the glycosyl side chain.[54,79] However, a recent study has revealed that MUC5AC, the primary type of mucin in human airway mucus, will undergo a charge transition between acidic and alkaline pH.[74] In the present study, this pH-dependent conformation and charge transition were observed. The circular dichroism (CD) analysis revealed that mucin was dominated by the random coil conformation,[77] and the pH-dependent intensity and width changes at 206 nm were observed (Figure S6), suggesting the conformation undergoes a transition from isotropic random coil to anisotropic extended random coil with the decrease of pH values.[77,80] Additionally, the mucin fiber in an acidic environment exhibited an increased zeta potential (Figure 4(e)), thus enhancing electrostatic interactions between

https://doi.org/10.1021/acsnano.2c11147
ACS Nano 2023, 17, 2813−2828

mucin fibers, increasing the viscosity of the mucus,[81] and inhibiting the movement of the particles. To study the transport behavior of particles in a pathological mucus environment, a mouse asthma model was established. Although this model could not restore the properties of acidic mucus (pH = 5.2) under the extreme pathological state (exacerbation of asthma), it confirmed that surface ligand type- and density-dependent mucus movement behavior was also shown (Figure 6(c)). Therefore, in addition to the changes in mucus pH, the effects of the content of mucin,[74] ion concentration,[74,82] and microorganisms[83] in mucus under physiological and pathological conditions on the carrier particle trans-mucus barrier deserve systematic and in-depth study.

Another focus during mucus penetration is the physicochemical properties of the carrier particles. A recent study has suggested that amine- and carboxyl-modified NPs were trapped in mucus due to noncovalent bond interactions such as electrostatic adsorption between the particle surface and mucin.[11] Notably, the present study demonstrated that these interfacial interactions were a function of the type and density of particle-surface-modified ligand. When SNPs were showing similar ligand densities, PEG- and amine-modified surfaces exhibited pH-independent mucus penetration and penetration inhibition, respectively. These are the reasons that PEGylated particles are widely regarded as mucus-penetrating particles (MPPs).[14,84,85] Additionally, the relationship between PEG modification density and mucus penetration has been reported. High-density PEG can shield the exposure of the particle core and improve the mucus penetration ability.[18] A recent study has designed a hierarchical PEG structure by optimizing the density and conformation of PEG on the surface of nanoparticles and revealed the protein adsorption kinetics. These "slippery nanoparticles" were used to reduce cell uptake[86] and the mucus penetration process,[87] which was consistent with the analysis in this study that the SNP−mucin interaction was shielded by regulating the PEG density and conformation (Figure 4(f,g)). Interestingly, the density-dependent fate of carboxyl-modified particles in mucus is unexpected. In neutral mucus, SNPs with 24.19 μmoL/m^2 of carboxyl were trapped in the mucus, but SNPs with 2.48 μmoL/m^2 of surface carboxyls exhibited a mucus-penetrating property (Figures 2 and 3). An existing study has also shown that although both carboxylated polystyrene (PS-COOH) and acid-terminated poly(lactide-*co*-glycolide) (PLGA) NPs showed mucoadhesive properties compared to PEG-modified NPs, there were differences in their motility in mucus. The effective diffusivity of PLGA was 2.3 times higher than that of PS-COOH nanoparticles,[88] which has been suggested to be related to the lower carboxyl density on the PLGA particle surface.[89] Furthermore, carboxyl-SNPs exhibited the advantage of mucus penetration only in a weakly alkaline environment, which was due to the changes of mucus properties as described above and the NPs−mucin interaction that will be discussed below.

The physicochemical property-dependent mucus penetration behavior was due to the interaction between SNPs and mucin, which has been studied by using molecular dynamics (MD)[49,90,91] simulation and experimental characterization.[82] However, systematic studies on the interaction mechanism between NPs' surface properties and mucin are currently missing. In this study, ITC was used to quantify thermodynamic parameters at the molecular level. Independent of mucin solution pH values and SNPs' surface ligand, the SNPs−mucin interaction was an enthalpy-driven process (Figure 5 and Table 1), indicating a noncovalent bond-mediated complex formation.[92] Notably, although high-density PEG-modified SNPs exhibited the lowest mucin binding strength (K_a = 0.14 × 10^8), a relatively high enthalpy change (1350 ± 283 kJ/mol) and entropy loss (−4392 ± 950 J/moL·K) were observed. It suggested that the thermodynamic characteristics of SNPs−mucin complexation were the equilibrium outcomes of noncovalent bond formation and solvent reorganization.[93] The PEGylated SNPs and mucin interaction-induced enthalpy change was the compensatory outcome of unfavorable desolvation enthalpy and favorable intrinsic enthalpy,[94] and the entropy loss was due to solute freedom reduction.[93] It was interesting to note that in an acidic environment, although both carboxyl and amino-SNPs were trapped in mucus (Figure 2), the K_a of carboxyl SNPs−mucin was significantly higher than that of amine-SNPs (Table 1), which may be explained by the fact that the carboxyl−mucin interactions were mainly dependent on hydrogen bonding. It has been suggested that an acidic environment was more conducive to the formation of hydrogen bonds between a carboxyl group and mucin,[95] and the hydrogen bonds were the predominant factor that governed the NPs−mucin interaction.[91,96]

In addition to the mucus penetration, the epithelial cell layer is another hurdle for drug carriers to overcome the mucosal barrier. Particles with a hydrophobic and positively charged surface are favorable for epithelium internalization due to enhanced interaction with cell membranes.[97,98] In this study, BEAS-2B cells were selected as model cells to study the uptake of engineered nanoparticles.[99,100] The MTS analysis showed that SNPs did not induce significant cytotoxicity (Figure S7) in BEAS-2B cells. The amine-modified SNPs could promote cellular uptake due to the stronger affinity between the positively charged surface and the cell membrane.[101] In contrast, the carboxyl and PEG modification led to decreased uptake (Figures S8 and S9). Interestingly, it was noticed that the PEG-modified SNPs exhibited better mucus penetration properties than amine and carboxyl modifications, but their cellular uptake ability was significantly inhibited. Breakthrough strategies with simultaneous mucus penetration and epithelial cell uptake have been developed.[66,67] Nanoparticle surface modification with polydopamine (PDA),[66] core−shell structure,[102] and viral biomimetic strategies[103] has recently been proposed to address the mucosal barrier. However, the composition of the mucus microenvironment, the regulation of NP surface modification, the mechanism of action at the NPs−mucin interface, and the modulation of downstream biological activity response deserve further exploration.

CONCLUSION

In this study, by using a comprehensive library of silica nanoparticles and MPT technology, it is demonstrated that surface properties are critical factors in determining the fate of particles during mucus penetration, which is affected by the mucus pH microenvironments, the type of surface modification, and the ligand density of NPs. The acidic mucus environment promotes the interaction between NPs and mucin due to strong mucus cross-linking and changed NP surface properties. Compared to amine- and carboxyl-modification, the PEG-SNPs exhibit stronger mucus penetration ability. Furthermore, the ligand-density-dependent mucus penetration was observed. This surface engineering approach provides a mechanistic understanding of the nanoparticle mucus penetration, which could be valuable in the design of drug delivery systems to other

https://doi.org/10.1021/acsnano.2c11147
ACS Nano 2023, 17, 2813−2828

mucosal systems, such as the eye, nasal cavity, gastrointestinal tract, and the female vagina.

MATERIALS AND METHODS

Reagents and Materials. Tetraethyl orthosilicate (TEOS), alginic acid sodium salt (AIg), D-(+)-gluconic acid δ-lactone (GDL), and mucin (from porcine stomach, Type II) were purchased from Sigma Aldrich (St. Louis, MO, USA). (3-Aminopropyl)triethoxysilane (APTEs) and 3-aminopropyl(diethoxy)methylsilane (APDEs) were purchased from Macklin (Shanghai, China). Ammonia solution (ACS, 28.0−30%), pyrocatechol violet (PV), and nickel chloride standard (0.5 M) were purchased from Aladdin (Shanghai, China). MOPS sodium salt, MOPS (free acid), sodium chloride, and calcium carbonate (anhydrous) were purchased from Sangon Biotech (Shanghai, China). The bicinchoninic acid (BCA) protein assay kit, HEPES buffer solution (1 M), Hoechst 33342, and wheat germ agglutinin 594 (WGA-594) were purchased from Thermo Fisher Scientific (OR, USA). Fluorescein isothiocyanate isomer I was purchased from Innochem (Beijing, China). 3-Aminopropyldimethylmethoxysilane (APEs) was purchased from Fluorochem (Derbyshire UK). Polyethylene glycol silane with a methoxyl terminus (mPEG-silane, 2K) was purchased from Huateng Pharma (Changsha, China). [(3-Triethoxysilyl)propyl]succinic anhydride (TESPSA) was purchased from TCI (Shanghai, China). Sodium acetate anhydrous was purchased from Damao (Tianjin, China).

Preparation of FITC-Labeled Stöber Silica Nanoparticles. The FITC-labeled silica nanoparticles were prepared with the Stöber method.[104] Briefly, FITC and APTEs were mixed in the ethanol and incubated with a digital shaking drybath for 1 h to prepare a FITC−APTEs solution. Then, ethyl alcohol (11 mL), deionized water (0.5 mL), ammonia solution (15 mL), and a FITC−APTEs solution (0.4 mL) were mixed at room temperature. Then, ethyl alcohol (80 mL) and TEOS (3 mL) were mixed and reacted for 16 h. The FITC-labeled Stöber silica nanoparticles were washed three times with deionized water and kept in deionized water before use.

Preparation of Silica Nanoparticles with Controlled Surface Modification. The low-, middle-, and high-density amine modifications on silica nanoparticles were prepared with APEs, APDEs, and APTEs, respectively. In a typical reaction, 100 mg of silica nanoparticles was dispersed into 10 mL of methanol, and the pH was adjusted to 3.0 with nitric acid (65−68%, wt %). Then the mixture was acidified at 40 °C. After 2 h, 0.3 mL of APEs, APDEs, and APTEs was added into the suspension for 4 h, respectively. The surface carboxyl modification on silica nanoparticles with different density was prepared with TESPSA. Briefly, for the low-density carboxyl group modification, 100 mg of silica nanoparticles was dispersed into 50 mL of ethyl alcohol, 20 μL of TESPSA (0.04%, v/v) was added into the flask for 30 min at 30 °C, and the mixture was reacted for 90 min at 30 °C. The middle-density (0.08%, v/v, and 40 °C), high-density (0.15%, v/v, and 80 °C), and HH-density (0.15%, v/v, and 120 °C) carboxyl modifications were prepared by adjusting the concentration of TESPSA and final reaction temperature accordingly. The surface PEG modifications on silica nanoparticles with different density were prepared with mPEG-silane. For the low- and high-density carboxyl group modification, 100 mg of silica nanoparticles was dispersed into 25 mL of ethyl alcohol, and 100 mg of mPEG-silane was dissolved into 25 mL of ethyl alcohol and mixed in the flask under magnetic agitation for 30 min at 30 °C; the mixture was reacted for 90 min at 80 °C (the high-density modification was 120 °C). The middle-density carboxyl group modification was the same as the amino group modification. A 100 mg amount of silica nanoparticles was dispersed into 10 mL of ethyl alcohol, and the pH values were adjusted to 3.0 with nitric acid (65−68%, wt %). Then the mixture was acidified at 40 °C. After 2 h, 50 mg of mPEG-silane was dissolved into 10 mL of ethyl alcohol and was poured into the flask to react for 4 h. All modified nanoparticles were washed three times with deionized water and kept in deionized water before use. The quantification analysis of surface moiety densities was determined as previously described.[38] The hydrodynamic sizes, PDI, and zeta potentials of silica nanoparticles were determined by a dynamic light scattering nanoparticle size analyzer (90Plus Zeta, Brookhaven, USA). The morphology and primary size of silica nanoparticles were determined by transmission electron microscopy (JEM-2100, JEOL, Japan).

PEG Conformation Analysis. The PEG conformation analysis was determined by calculating the Flory radius (R_F), the distance (D) between the PEG graft sites, and the thickness (L) of the grafted PEG layer.[55] The R_F is related to the number and length of the monomer units, and it could be calculated as

$$R_F = \alpha N^{3/5}$$

The D was calculated as

$$D = 2\sqrt{\frac{A}{\pi}}$$

The L was calculated as

$$L = \frac{N\alpha^{5/3}}{D^{2/3}}$$

where α is the length of the ethoxy unity and N is the extent of polymerization of PEG. For the PEG_{2k}, α is 0.35 nm and N is 44.44. A is the area occupied by the PEG chain on the silica nanoparticle.

Preparation of Artificial Airway Mucus. The preparation of artificial airway mucus was performed as previously described.[45] The mucin and sodium salt of AIg were dissolved in ultrapure water under magnetic agitation overnight. On the day of the experiment, the mucin solution (43.75 mg/mL), sodium salt solution of calcium carbonate (14 mg/mL), GDL (49.84 mg/mL), and AIg (21 mg/mL) were mixed in a reaction flask under magnetic agitation for 1 min. The pH was adjusted with a 1 M sodium hydroxide solution.

Rheological Characterization of Artificial Mucus. Rheological measurements were performed by a rotational rheometer (MCR302, Anton Paar, Austria) equipped with a double-gap measuring system at 25 °C. The viscosity was determined at the shear rate $1-10^3$ 1/s to cover mucus shear states during static breathing (0.5 1/s)[45] and dynamic coughing (10^3-10^4 1/s).[105] The linear viscoelastic region of artificial mucus was determined by a strain sweep test from the strain range of $0.1-10^3$%. The storage component (G', Pa) and loss component (G'', Pa) of artificial mucus were evaluated by oscillatory frequency sweep measurements at a 0.5% strain amplitude (according to strain sweep results), and the frequency range was set at 0.05−1.6 Hz to include the normal breathing rate (0.5 Hz).[45]

Collection of Native Mucus Samples. Specific pathogen-free (SPF) CD rats (female, 6−8 weeks) were purchased from Liaoning Changsheng Biotechnology Co., Ltd. All animal protocols were approved by the Animal Research Committee at the Dalian University of Technology. Animals were prefasted for 1 day and then sacrificed. The ileum was removed intact and gently flushed with ice-cold saline. The ileum was axially dissected and fixed, and the intestinal surface mucus was gently scraped with a small spatula and collected into a centrifuge tube. The native mucus samples were stored at −80 °C before use.

Multiple Particle Tracking. The multiple particle motion trajectory in mucus was recorded by a CCD camera (Leica DFC9000 GT, Germany) mounted on a fluorescent inverted microscope with a 100× oil-immersion objective (Leica DMi8, Germany). FITC-labeled silica nanoparticles (0.4 mg/mL) were added to mucus with different pH values in eight-well chambers at a final concentration of 3% (v/v). Prior to MPT, the mucus−nanoparticle system was incubated for 2 h at 37 °C to eliminate the influence of fluid flow on particle movement. Movies were captured for 20 s (total frames = 300) and analyzed by a custom-written program in MATLAB (MathWorks, Natick, MA, USA), which was based on the algorithm of Crocker and Grier.[106] At least 200 particles were tracked in each sample, and at least 25 frames were analyzed from each tracking. Sample video files are provided in Supporting Information Videos S1−S5.

The ensemble MSD was calculated as

$$\mathrm{MSD} = \langle \Delta r^2(\tau) \rangle = \langle [X(t+\tau) - X(t)]^2 + [Y(t+\tau) - Y(t)]^2 \rangle$$

The effective diffusivity (D_{eff}) can be obtained by

https://doi.org/10.1021/acsnano.2c11147
ACS Nano 2023, 17, 2813−2828

$$D_{\text{eff}} = \frac{\langle \Delta r^2(\tau) \rangle}{4\tau}$$

The anomalous exponent (α) is defined as

$$\alpha = \frac{d \log(\Delta r^2(\tau))}{d \log(\tau)}$$

Isothermal Titration Calorimeter Characterization. The interaction between mucin and nanoparticles was characterized by nano ITC (TA Instruments, USA). Prior to titration, the mucin solution was centrifuged at 8000 rpm for 40 min at 4 °C, and the supernatant was collected. Then, the supernatant was dialyzed to pH 5.2, pH 7.0 (20 mM NaAc buffer), and pH 7.7 (20 mM MOPS buffer), respectively. The mucin with different pH values was lyophilized, and mucin quantification was performed by a BCA protein assay kit. In order to eliminate the interference of chemical potential, the surface-modified silica nanoparticles were also resuspended in the buffer solution of the same pH values. All samples were degassed under vacuum for 10 min to prevent bubbling. Then 50 μL of mucin solution (0.004 mM) was injected into 300 μL of nanoparticle solution (10 mg/mL), and each injection interval was 300 s (total number = 25) with stirring (300 rpm) to ensure proper mixing after each injection. The temperature was set to 25 °C. All ITC data were analyzed using the NanoAnalyze Data Analysis software, version 3.11.0 (TA Instruments), and the first injection was ignored.

Distribution of Nanoparticles in the Mouse Airway. SPF Balb/c and C57BL/6 mice (female, 6−8 weeks) were purchased from Liaoning Changsheng Biotechnology Co., Ltd. All animal protocols were approved by the Animal Research Committee at the Dalian University of Technology. The OVA-asthma mouse model was constructed based on previously published studies.[107] Briefly, C57BL/6 mice were sensitized by intraperitoneal injection of aluminum hydroxide solution of ovalbumin (OVA) (75 μg of OVA and 2 mg of aluminum hydroxide in 200 μL of PBS) on day 1 and 8. Then, 50 μg of OVA was delivered through intranasal administration on day 15, 16, and 17, respectively. Surface-modified silica nanoparticles were then intratracheally administrated on day 18 to study the distribution of nanoparticles in the mouse airway. The airway distribution studies were performed based on previously published studies.[26] Briefly, the mice were anesthetized with intraperitoneal injection of pentobarbital sodium, and 50 μL of FITC-labeled silica nanoparticles with controlled surface modification was resuspended in PBS and intratracheally administrated. After 30 min, mice were sacrificed to collect the lungs, which were further fixed in 4% PFA, embedded with optimum cutting temperature (OCT) compound, and cryosectioned. The sections were stained with Hoechst 33342 and observed with a fluorescent inverted microscope (Leica DMi8, Germany).

BEAS-2B Cell Culture and Cytotoxicity Assessment. BEAS-2B cells were grown in Dulbecco's modified Eagle medium (DMEM) supplemented with 10% fetal bovine serum and penicillin (100 U/mL)−streptomycin (100 mg/mL). The MTS assay was used to evaluate the viabilities of BEAS-2B cells. Cells were seeded in a 96-well plate at a density of 3×10^4 cells/well for 12 h at 37 °C and 5% CO_2. Then the surface-modified silica nanoparticles were added to cells at a concentrations range of 12.5−200 μg/mL for 24 h. The medium was removed, and the MTS solution/culture medium (1:5) was added to wells for 40 min at 37 °C. The supernatant was used to detect the absorbance value under 490 nm light.

Cellular Uptake of Silica Nanoparticles. BEAS-2B cells were seeded in an eight-well chamber at 1.5×10^5 cells/well for 12 h at 37 °C and 5% CO_2. Cells were treated with FITC-labeled silica nanoparticles (25 μg/mL) for 12 h at 37 °C. Then the cells were fixed with 4% PFA for 20 min at room temperature and then were stained with WGA Alexa Fluor 594 conjugate (1 μg/mL) and Hoechst 33342 (10 μm) for 20 min at room temperature. Finally, the cells were examined using a confocal microscope (Olympus, FV1000). For the quantitative analysis of cellular uptake, BEAS-2B cells were seeded in a 24-well plate with a density of 2.5×10^5 cells/well and grown for 12 h at 37 °C and 5% CO_2. Cells were treated with 25 μg/mL FITC-labeled silica nanoparticles for 2 h at 37 °C. Then the culture media was removed, and cells were washed three times with PBS to remove noninternalized nanoparticles. Cells were detached using 150 μL of 0.25% trypsin-EDTA solution at 37 °C for 5 min. Then, cells were washed two times with FACS (1% FBS in DPBS) buffer and analyzed by flow cytometry (Accuri C6 Plus, BD). Trypan blue was used to quench the fluorescence associated with the cell surface.[108]

Statistical Analysis. For all the figures without special instructions, the values shown represent mean ± SD. The two-tailed t test analysis was used to determine significant differences between two groups. p values are shown in figure legends. Differences were considered to be statistically significant at a level of $p < 0.05$.

ASSOCIATED CONTENT

Supporting Information

The Supporting Information is available free of charge at https://pubs.acs.org/doi/10.1021/acsnano.2c11147.

Additional rheological characterization data of artificial mucus and comparative analysis with rheological properties of real airway mucus; hydrodynamic sizes, ζ potentials of FITC-labeled and pristine SNPs; representative trajectories, ensemble mean squared displacement, logarithms of effective diffusivities, and anomalous exponent of pristine and HH-COOH SNPs; quantitative analysis of carboxyl density on HH-COOH SNPs; CD spectra of mucin dialysis solutions at different pH values; toxicity assessment and cellular uptake of surface-engineered SNPs with BEAS-2B cells (PDF)

Movies of surface-engineered SNPs' motility behavior in artificial and rat ileum mucus (ZIP)

AUTHOR INFORMATION

Corresponding Author

Bingbing Sun − *State Key Laboratory of Fine Chemicals, Dalian University of Technology, 116024 Dalian, China; School of Chemical Engineering, Dalian University of Technology, 116024 Dalian, China;* orcid.org/0000-0002-5444-5078; Email: bingbingsun@dlut.edu.cn

Authors

Yiyang Guo − *State Key Laboratory of Fine Chemicals, Dalian University of Technology, 116024 Dalian, China; School of Chemical Engineering, Dalian University of Technology, 116024 Dalian, China*

Yubin Ma − *State Key Laboratory of Fine Chemicals, Dalian University of Technology, 116024 Dalian, China; School of Chemical Engineering, Dalian University of Technology, 116024 Dalian, China*

Xin Chen − *School of Chemical Engineering, Dalian University of Technology, 116024 Dalian, China*

Min Li − *State Key Laboratory of Fine Chemicals, Dalian University of Technology, 116024 Dalian, China; School of Chemical Engineering, Dalian University of Technology, 116024 Dalian, China;* orcid.org/0000-0002-7966-9297

Xuehu Ma − *School of Chemical Engineering, Dalian University of Technology, 116024 Dalian, China;* orcid.org/0000-0002-9496-3734

Gang Cheng − *Department of Chemical Engineering, University of Illinois at Chicago, Chicago, Illinois 60607, United States;* orcid.org/0000-0002-7170-8968

Changying Xue − *School of Bioengineering, Dalian University of Technology, 116024 Dalian, China*

https://doi.org/10.1021/acsnano.2c11147
ACS Nano 2023, 17, 2813−2828

Yi Y. Zuo − *Department of Mechanical Engineering, University of Hawaii at Manoa, Honolulu, Hawaii 96822, United States;* orcid.org/0000-0002-3992-3238

Complete contact information is available at: https://pubs.acs.org/10.1021/acsnano.2c11147

Author Contributions

B.S. and Y.G. conceived the study and designed the experiments. Y.G., Y.M., and X.C. performed the experiments. Y.G., Y.M., M.L., X.M., C.X., G.C., Y.Z., and B.S. analyzed the data and contributed to writing of the manuscript. All authors contributed to the manuscript and approved the final version of the manuscript.

Notes

The authors declare no competing financial interest.

ACKNOWLEDGMENTS

This work was supported by the National Key Research and Development Program of China (2022YFC2304305), the National Natural Science Foundation of China (31870919 and 21876017), Natural Science Foundation of Liaoning Province (XLYC1807113), Dalian Science and Technology Innovation Fund (2020JJ25CY015), and Fundamental Research Funds for the Central Universities (DUT21ZD216). Special thanks to Dr. Yongning Bian and Dr. Wei Zhang (State Key Laboratory of Structure Analysis for Industrial Equipment, Department of Engineering Mechanics, Dalian University of Technology) for help with rheological characterization of mucus.

REFERENCES

(1) Wan, F.; Bohr, S. S. R.; Klodzinska, S. N.; Jumaa, H.; Huang, Z.; Nylander, T.; Thygesen, M. B.; Sorensen, K. K.; Jensen, K. J.; Sternberg, C.; Hatzakis, N.; Nielsen, H. M. Ultrasmall TPGS-PLGA Hybrid Nanoparticles for Site-Specific Delivery of Antibiotics into Pseudomonas aeruginosa Biofilms in Lungs. *ACS Appl. Mater. Interfaces.* **2020**, *12*, 380−389.

(2) Li, Z.; Luo, G.; Hu, W.; Hua, J.; Geng, S.; Chu, P.; Zhang, J.; Wang, H.; Yu, X. Mediated Drug Release from Nanovehicles by Black Phosphorus Quantum Dots for Efficient Therapy of Chronic Obstructive Pulmonary Disease. *Angew. Chem., Int. Ed.* **2020**, *59*, 20568−20576.

(3) Da Silva, A. L.; De Oliveira, G. P.; Kim, N.; Cruz, F. F.; Kitoko, J. Z.; Blanco, N. G.; Martini, S. V.; Hanes, J.; Rocco, P. R. M.; Suk, J. S.; Morales, M. M. Nanoparticle-based thymulin gene therapy therapeutically reverses key pathology of experimental allergic asthma. *Sci. Adv.* **2020**, *6*, No. eaay7973.

(4) Khurana, A.; Allawadhi, P.; Khurana, I.; Allwadhi, S.; Weiskirchen, R.; Banothu, A. K.; Chhabra, D.; Joshi, K.; Bharani, K. K. Role of nanotechnology behind the success of mRNA vaccines for COVID-19. *Nano Today.* **2021**, *38*, 101142.

(5) Chauhan, G.; Madou, M. J.; Kalra, S.; Chopra, V.; Ghosh, D.; Martinez-Chapa, S. O. Nanotechnology for COVID-19: Therapeutics and Vaccine Research. *ACS Nano* **2020**, *14*, 7760−7782.

(6) Cone, R. A. Barrier properties of mucus. *Adv. Drug Delivery Rev.* **2009**, *61*, 75−85.

(7) Dong, W.; Ye, J.; Zhou, J.; Wang, W.; Wang, H.; Zheng, X.; Yang, Y.; Xia, X.; Liu, Y. Comparative study of mucoadhesive and mucus-penetrative nanoparticles based on phospholipid complex to overcome the mucus barrier for inhaled delivery of baicalein. *Acta Pharm. Sin. B* **2020**, *10*, 1576−1585.

(8) Song, D.; Cahn, D.; Duncan, G. A. Mucin Biopolymers and Their Barrier Function at Airway Surfaces. *Langmuir.* **2020**, *36*, 12773−12783.

(9) Murgia, X.; Loretz, B.; Hartwig, O.; Hittinger, M.; Lehr, C. M. The role of mucus on drug transport and its potential to affect therapeutic outcomes. *Adv. Drug Delivery Rev.* **2018**, *124*, 82−97.

(10) Bandi, S. P.; Kumbhar, Y. S.; Venuganti, V. V. K. Effect of particle size and surface charge of nanoparticles in penetration through intestinal mucus barrier. *J. Nanopart. Res.* **2020**, *22*, 62.

(11) Liu, Q.; Guan, J.; Qin, L.; Zhang, X.; Mao, S. Physicochemical properties affecting the fate of nanoparticles in pulmonary drug delivery. *Drug Discovery Today.* **2020**, *25*, 150−159.

(12) Liu, Q.; Guan, J.; Song, R.; Zhang, X.; Mao, S. Physicochemical properties of nanoparticles affecting their fate and the physiological function of pulmonary surfactants. *Acta Biomater.* **2022**, *140*, 76−87.

(13) Liu, M.; Zhang, J.; Shan, W.; Huang, Y. Developments of mucus penetrating nanoparticles. *Asian J. Pharm. Sci.* **2015**, *10*, 275−282.

(14) Huckaby, J. T.; Lai, S. K. PEGylation for enhancing nanoparticle diffusion in mucus. *Adv. Drug Delivery Rev.* **2018**, *124*, 125−139.

(15) Schneider, C. S.; Xu, Q.; Boylan, N. J.; Chisholm, J.; Tang, B. C.; Schuster, B. S.; Henning, A.; Ensign, L. M.; Lee, E.; Adstamongkonkul, P. Nanoparticles that do not adhere to mucus provide uniform and long-lasting drug delivery to airways following inhalation. *Sci. Adv.* **2017**, *3*, No. e1601556.

(16) Maisel, K.; Reddy, M.; Xu, Q.; Chattopadhyay, S.; Cone, R.; Ensign, L. M.; Hanes, J. Nanoparticles coated with high molecular weight PEG penetrate mucus and provide uniform vaginal and colorectal distribution in vivo. *Nanomedicine.* **2016**, *11*, 1337−1343.

(17) Samaridou, E.; Kalamidas, N.; Santalices, I.; Crecente-Campo, J.; Alonso, M. J. Tuning the PEG surface density of the PEG-PGA enveloped Octaarginine-peptide Nanocomplexes. *Drug Deliv Transl Res.* **2020**, *10*, 241−258.

(18) Xu, Q.; Ensign, L. M.; Boylan, N. J.; Schon, A.; Gong, X.; Yang, J.; Lamb, N. W.; Cai, S.; Yu, T.; Freire, E.; Hanes, J. Impact of Surface Polyethylene Glycol (PEG) Density on Biodegradable Nanoparticle Transport in Mucus ex Vivo and Distribution in Vivo. *ACS Nano* **2015**, *9*, 9217−9227.

(19) Poinard, B.; Kamaluddin, S.; Tan, A. Q. Q.; Neoh, K. G.; Kah, J. C. Y. Polydopamine Coating Enhances Mucopenetration and Cell Uptake of Nanoparticles. *ACS Appl. Mater. Interfaces.* **2019**, *11*, 4777−4789.

(20) Zhou, Y.; Chen, Z.; Zhao, D.; Li, D.; He, C.; Chen, X. A pH-Triggered Self-Unpacking Capsule Containing Zwitterionic Hydrogel-Coated MOF Nanoparticles for Efficient Oral Exendin-4 Delivery. *Adv. Mater.* **2021**, *33*, No. e2102044.

(21) Rao, R.; Liu, X.; Li, Y.; Tan, X.; Zhou, H.; Bai, X.; Yang, X.; Liu, W. Bioinspired zwitterionic polyphosphoester modified porous silicon nanoparticles for efficient oral insulin delivery. *Biomater Sci.* **2021**, *9*, 685−699.

(22) Zhang, Y.; Xiong, M.; Ni, X.; Wang, J.; Rong, H.; Su, Y.; Yu, S.; Mohammad, I. S.; Leung, S. S. Y.; Hu, H. Virus-Mimicking Mesoporous Silica Nanoparticles with an Electrically Neutral and Hydrophilic Surface to Improve the Oral Absorption of Insulin by Breaking Through Dual Barriers of the Mucus Layer and the Intestinal Epithelium. *ACS Appl. Mater. Interfaces.* **2021**, *13*, 18077−18088.

(23) Han, X.; Lu, Y.; Xie, J.; Zhang, E.; Zhu, H.; Du, H.; Wang, K.; Song, B.; Yang, C.; Shi, Y.; Cao, Z. Zwitterionic micelles efficiently deliver oral insulin without opening tight junctions. *Nat. Nanotechnol.* **2020**, *15*, 605−614.

(24) Li, Y.; Ji, W.; Peng, H.; Zhao, R.; Zhang, T.; Lu, Z.; Yang, J.; Liu, R.; Zhang, X. Charge-switchable zwitterionic polycarboxybetaine particle as an intestinal permeation enhancer for efficient oral insulin delivery. *Theranostics.* **2021**, *11*, 4452−4466.

(25) Song, W.; Yang, Y.; Yu, M.; Zhu, Q.; Damaneh, M. S.; Zhong, H.; Gan, Y. Enhanced digestion inhibition and mucus penetration of F127-modified self-nanoemulsions for improved oral delivery. *Asian J. Pharm. Sci.* **2018**, *13*, 326−335.

(26) Leal, J.; Peng, X.; Liu, X.; Arasappan, D.; Wylie, D. C.; Schwartz, S. H.; Fullmer, J. J.; McWilliams, B. C.; Smyth, H. D. C.; Ghosh, D. Peptides as surface coatings of nanoparticles that penetrate human cystic fibrosis sputum and uniformly distribute in vivo following pulmonary delivery. *J. Controlled Release* **2020**, *322*, 457−469.

(27) Wang, A.; Yang, T.; Fan, W.; Yang, Y.; Zhu, Q.; Guo, S.; Zhu, C.; Yuan, Y.; Zhang, T.; Gan, Y. Protein Corona Liposomes Achieve Efficient Oral Insulin Delivery by Overcoming Mucus and Epithelial Barriers. *Adv. Healthcare Mater.* **2019**, *8*, 1801123.
(28) Hill, D. B.; Button, B.; Rubinstein, M.; Boucher, R. C. Physiology and pathophysiology of human airway mucus. *Physiol Rev.* **2022**, *102*, 1757−1836.
(29) Leal, J.; Smyth, H. D. C.; Ghosh, D. Physicochemical properties of mucus and their impact on transmucosal drug delivery. *Int. J. Pharm.* **2017**, *532*, 555−572.
(30) Ricciardolo, F. L. M.; Gaston, B.; Hunt, J. Acid stress in the pathology of asthma. *J. Allergy Clin. Immunol.* **2004**, *113*, 610−619.
(31) Hunt, J. F.; Fang, K.; Malik, R.; Snyder, A.; Malhotra, N.; Platts-Mills, T. A. E.; Gaston, B. Endogenous airway acidification - Implications for asthma pathophysiology. *Am. J. Respir. Crit. Care Med.* **2000**, *161*, 694−699.
(32) Zajac, M.; Dreano, E.; Edwards, A.; Planelles, G.; Sermet-Gaudelus, I. Airway Surface Liquid pH Regulation in Airway Epithelium Current Understandings and Gaps in Knowledge. *Int. J. Mol. Sci.* **2021**, *22*, 3384.
(33) Ruiz-Pulido, G.; Medina, D. I. An overview of gastrointestinal mucus rheology under different pH conditions and introduction to pH-dependent rheological interactions with PLGA and chitosan nanoparticles. *Eur. J. Pharm. Biopharm.* **2021**, *159*, 123−136.
(34) Parlato, R. M.; Greco, F.; Maffettone, P. L.; Larobina, D. Effect of pH on the viscoelastic properties of pig gastric mucus. *J. Mech. Behav. Biomed. Mater.* **2019**, *98*, 195−199.
(35) Deirram, N.; Zhang, C. H.; Kermaniyan, S. S.; Johnston, A. P. R.; Such, G. K. pH-Responsive Polymer Nanoparticles for Drug Delivery. *Macromol. Rapid Commun.* **2019**, *40*, 1800917.
(36) Das Neves, J.; Amiji, M.; Sarmento, B. Mucoadhesive nanosystems for vaginal microbicide development: friend or foe? *Wiley Interdiscip. Rev.: Nanomed. Nanobiotechnol.* **2011**, *3*, 389−399.
(37) Zhang, T.; Zhang, Q.; Ge, J.; Goebl, J.; Sun, M.; Yan, Y.; Liu, Y.; Chang, C.; Guo, J.; Yin, Y. A Self-Templated Route to Hollow Silica Microspheres. *J. Phys. Chem. C* **2009**, *113*, 3168−3175.
(38) Li, M.; Cheng, F.; Xue, C.; Wang, H.; Chen, C.; Du, Q.; Ge, D.; Sun, B. Surface Modification of Stober Silica Nanoparticles with Controlled Moiety Densities Determines Their Cytotoxicity Profiles in Macrophages. *Langmuir.* **2019**, *35*, 14688−14695.
(39) Bozuyuk, U.; Dogan, N. O.; Kizilel, S. Deep Insight into PEGylation of Bioadhesive Chitosan Nanoparticles: Sensitivity Study for the Key Parameters Through Artificial Neural Network Model. *ACS Appl. Mater. Interfaces.* **2018**, *10*, 33945−33955.
(40) Rahme, K.; Chen, L.; Hobbs, R. G.; Morris, M. A.; O'Driscoll, C.; Holmes, J. D. PEGylated gold nanoparticles: polymer quantification as a function of PEG lengths and nanoparticle dimensions. *RSC Adv.* **2013**, *3*, 6085−6094.
(41) Zhang, M.; Lei, J.; Shi, Y.; Zhang, L.; Ye, Y.; Li, D.; Mu, C. Molecular weight effects of PEG on the crystal structure and photocatalytic activities of PEG-capped TiO2 nanoparticles. *RSC Adv.* **2016**, *6*, 83366−83372.
(42) Shah, V. S.; Meyerholz, D. K.; Tang, X.; Reznikov, L.; Abou Alaiwa, M.; Ernst, S. E.; Karp, P. H.; Wohlford-Lenane, C. L.; Heilmann, K. P.; Leidinger, M. R.; Allen, P. D.; Zabner, J.; McCray, P. B.; Ostedgaard, L. S.; Stoltz, D. A.; Randak, C. O.; Welsh, M. J. Airway acidification initiates host defense abnormalities in cystic fibrosis mice. *Science.* **2016**, *351*, 503−507.
(43) Abou Alaiwa, M. H.; Launspach, J. L.; Grogan, B.; Carter, S.; Zabner, J.; Stoltz, D. A.; Singh, P. K.; McKone, E. F.; Welsh, M. J. Ivacaftor-induced sweat chloride reductions correlate with increases in airway surface liquid pH in cystic fibrosis. *Jci Insight.* **2018**, *3*, No. e121468.
(44) Kim, D.; Liao, J.; Scales, N. B.; Martini, C.; Luan, X.; Abu-Arish, A.; Robert, R.; Luo, Y.; McKay, G. A.; Nguyen, D.; Tewfik, M. A.; Poirier, C. D.; Matouk, E.; Ianowski, J. P.; Frenkiel, S.; Hanrahan, J. W. Large pH oscillations promote host defense against human airways infection. *J. Exp Med.* **2021**, *218*, No. e20201831.
(45) Pacheco, D. P.; Butnarasu, C. S.; Vangosa, F. B.; Pastorino, L.; Visai, L.; Visentin, S.; Petrini, P. Disassembling the complexity of mucus barriers to develop a fast screening tool for early drug discovery. *J. Mater. Chem. B* **2019**, *7*, 4940−4952.
(46) Yuan, S.; Hollinger, M.; Lachowicz-Scroggins, M. E.; Kerr, S. C.; Dunican, E. M.; Daniel, B. M.; Ghosh, S.; Erzurum, S. C.; Willard, B.; Hazen, S. L.; Huang, X.; Carrington, S. D.; Oscarson, S.; Fahy, J. V. Oxidation increases mucin polymer cross-links to stiffen airway mucus gels. *Sci. Transl. Med.* **2015**, *7*, 276ra227.
(47) Suh, J.; Dawson, M.; Hanes, J. Real-time multiple-particle tracking: Applications to drug and gene delivery. *Adv. Drug Delivery Rev.* **2005**, *57*, 1551−1551.
(48) Abdulkarim, M.; Agullo, N.; Cattoz, B.; Griffiths, P.; Bernkop-Schnurch, A.; Borros, S.; Gumbleton, M. Nanoparticle diffusion within intestinal mucus: Three-dimensional response analysis dissecting the impact of particle surface charge, size and heterogeneity across polyelectrolyte, pegylated and viral particles. *Eur. J. Pharm. Biopharm.* **2015**, *97*, 230−238.
(49) Yu, M.; Xu, L.; Tian, F.; Su, Q.; Zheng, N.; Yang, Y.; Wang, J.; Wang, A.; Zhu, C.; Guo, S.; Zhang, X.; Gan, Y.; Shi, X.; Gao, H. Rapid transport of deformation-tuned nanoparticles across biological hydrogels and cellular barriers. *Nat. Commun.* **2018**, *9*, 2607.
(50) Huck, B. C.; Hartwig, O.; Biehl, A.; Schwarzkopf, K.; Wagner, C.; Loretz, B.; Murgia, X.; Lehr, C. M. Macro- and Microrheological Properties of Mucus Surrogates in Comparison to Native Intestinal and Pulmonary Mucus. *Biomacromolecules.* **2019**, *20*, 3504−3512.
(51) Murgia, X.; Pawelzyk, P.; Schaefer, U. F.; Wagner, C.; Willenbacher, N.; Lehr, C. M. Size-Limited Penetration of Nanoparticles into Porcine Respiratory Mucus after Aerosol Deposition. *Biomacromolecules.* **2016**, *17*, 1536−1542.
(52) Schuster, B. S.; Suk, J. S.; Woodworth, G. F.; Hanes, J. Nanoparticle diffusion in respiratory mucus from humans without lung disease. *Biomaterials.* **2013**, *34*, 3439−3446.
(53) Lai, S. K.; O'Hanlon, D. E.; Harrold, S.; Man, S. T.; Wang, Y.; Cone, R.; Hanes, J. Rapid transport of large polymeric nanoparticles in fresh undiluted human mucus. *Proc. Natl. Acad. Sci. U. S. A.* **2007**, *104*, 1482−1487.
(54) Jin, Q.; Zhu, W.; Zhu, J.; Zhu, J.; Shen, J.; Liu, Z.; Yang, Y.; Chen, Q. Nanoparticle-Mediated Delivery of Inhaled Immunotherapeutics for Treating Lung Metastasis. *Adv. Mater.* **2021**, *33*, No. e2007557.
(55) Perry, J. L.; Reuter, K. G.; Kai, M.; Herlihy, K. P.; Jones, S. W.; Luft, J. C.; Napier, M.; Bear, J. E.; DeSimone, J. M. PEGylated PRINT Nanoparticles: The Impact of PEG Density on Protein Binding, Macrophage Association, Biodistribution, and Pharmacokinetics. *Nano Lett.* **2012**, *12*, 5304−5310.
(56) Damodaran, V. B.; Fee, C. J.; Ruckh, T.; Popat, K. C. Conformational Studies of Covalently Grafted Poly(ethylene glycol) on Modified Solid Matrices Using X-ray Photoelectron Spectroscopy. *Langmuir.* **2010**, *26*, 7299−7306.
(57) Ba, X.; Gao, T.; Yang, M.; Jiang, P.; Liu, Y. Thermodynamics of the Interaction Between Graphene Quantum Dots with Human Serum Albumin and γ-Globulins. *J. Solution Chem.* **2020**, *49*, 100−116.
(58) Chakraborti, S.; Joshi, P.; Chakravarty, D.; Shanker, V.; Ansari, Z. A.; Singh, S. P.; Chakrabarti, P. Interaction of Polyethyleneimine-Functionalized ZnO Nanoparticles with Bovine Serum Albumin. *Langmuir.* **2012**, *28*, 11142−11152.
(59) Jayaraman, S.; Song, Y.; Vetrivel, L.; Shankar, L.; Verkman, A. S. Noninvasive in vivo fluorescence measurement of airway-surface liquid depth, salt concentration, and pH. *J. Clin. Invest.* **2001**, *107*, 317−324.
(60) Jayaraman, S.; Song, Y.; Verkman, A. S. Airway surface liquid pH in well-differentiated airway epithelial cell cultures and mouse trachea. *Am. J. Physiol.: Cell Physiol.* **2001**, *281*, C1504−C1511.
(61) Ma, J.; Rubin, B. K.; Voynow, J. A. Mucins, Mucus, and Goblet Cells. *Chest.* **2018**, *154*, 169−176.
(62) Sun, B.; Pokhrel, S.; Dunphy, D. R.; Zhang, H.; Ji, Z.; Wang, X.; Wang, M.; Liao, Y.; Chang, C.; Dong, J.; Li, R.; Madler, L.; Brinker, C. J.; Nel, A. E.; Xia, T. Reduction of Acute Inflammatory Effects of Fumed Silica Nanoparticles in the Lung by Adjusting Silanol Display through Calcination and Metal Doping. *ACS Nano* **2015**, *9*, 9357−9372.

https://doi.org/10.1021/acsnano.2c11147
ACS Nano 2023, 17, 2813−2828

(63) Sun, B.; Wang, X.; Liao, Y.; Ji, Z.; Chang, C.; Pokhrel, S.; Ku, J.; Liu, X.; Wang, M.; Dunphy, D. R.; Li, R.; Meng, H.; Maedler, L.; Brinker, C. J.; Nel, A. E.; Xia, T. Repetitive Dosing of Fumed Silica Leads to Profibrogenic Effects through Unique Structure-Activity Relationships and Biopersistence in the Lung. *ACS Nano* **2016**, *10*, 8054−8066.
(64) Netsomboon, K.; Bemkop-Schnurch, A. Mucoadhesive vs. mucopenetrating particulate drug delivery. *Eur. J. Pharm. Biopharm.* **2016**, *98*, 76−89.
(65) Wu, L.; Shan, W.; Zhang, Z.; Huang, Y. Engineering nanomaterials to overcome the mucosal barrier by modulating surface properties. *Adv. Drug Delivery Rev.* **2018**, *124*, 150−163.
(66) Hu, S.; Yang, Z.; Wang, S.; Wang, L.; He, Q.; Tang, H.; Ji, P.; Chen, T. Zwitterionic polydopamine modified nanoparticles as an efficient nanoplatform to overcome both the mucus and epithelial barriers. *Chem. Eng. J.* **2022**, *428*, 132107.
(67) Hu, S.; Pei, X.; Duan, L.; Zhu, Z.; Liu, Y.; Chen, J.; Chen, T.; Ji, P.; Wan, Q.; Wang, J. A mussel-inspired film for adhesion to wet buccal tissue and efficient buccal drug delivery. *Nat. Commun.* **2021**, *12*, 1689.
(68) Porsio, B.; Craparo, E. F.; Mauro, N.; Giammona, G.; Cavallaro, G. Mucus and Cell-Penetrating Nanoparticles Embedded in Nano-into-Micro Formulations for Pulmonary Delivery of Ivacaftor in Patients with Cystic Fibrosis. *ACS Appl. Mater. Interfaces.* **2018**, *10*, 165−181.
(69) Tang, B.; Dawson, M.; Lai, S. K.; Wang, Y.; Suk, J. S.; Yang, M.; Zeitlin, P.; Boyle, M. P.; Fu, J.; Hanes, J. Biodegradable polymer nanoparticles that rapidly penetrate the human mucus barrier. *Proc. Natl. Acad. Sci. U. S. A.* **2009**, *106*, 19268−19273.
(70) Suk, J. S.; Lai, S. K.; Wang, Y.; Ensign, L. M.; Zeitlin, P. L.; Boyle, M. P.; Hanes, J. The penetration of fresh undiluted sputum expectorated by cystic fibrosis patients by non-adhesive polymer nanoparticles. *Biomaterials.* **2009**, *30*, 2591−2597.
(71) Hunt, J. F.; Gaston, B. Airway acidification and gastroesophageal reflux. *Curr. Allergy Asthma Rep.* **2008**, *8*, 79−84.
(72) Kostikas, K.; Papatheodorou, G.; Ganas, K.; Psathakis, K.; Panagou, P.; Loukides, S. pH in expired breath condensate of patients with inflammatory airway diseases. *Am. J. Respir. Crit. Care Med.* **2002**, *165*, 1364−1370.
(73) Tate, S.; MacGregor, G.; Davis, M.; Innes, J. A.; Greening, A. P. Airways in cystic fibrosis are acidified: detection by exhaled breath condensate. *Thorax.* **2002**, *57*, 926−929.
(74) Lieleg, O.; Vladescu, I.; Ribbeck, K. Characterization of Particle Translocation through Mucin Hydrogels. *Biophys. J.* **2010**, *98*, 1782−1789.
(75) Curnutt, A.; Smith, K.; Darrow, E.; Walters, K. B. Chemical and Microstructural Characterization of pH and Ca2+ Dependent Sol-Gel Transitions in Mucin Biopolymer. *Sci. Rep.* **2020**, *10*, 8760.
(76) Celli, J. P.; Turner, B. S.; Afdhal, N. H.; Ewoldt, R. H.; McKinley, G. H.; Bansil, R.; Erramilli, S. Rheology of gastric mucin exhibits a pH-dependent sol-gel transition. *Biomacromolecules.* **2007**, *8*, 1580−1586.
(77) Bansil, R.; Turner, B. S. Mucin structure, aggregation, physiological functions and biomedical applications. *Curr. Opin. Colloid Interface Sci.* **2006**, *11*, 164−170.
(78) Lee, S.; Muller, M.; Rezwan, K.; Spencer, N. D. Porcine gastric mucin (PGM) at the water/poly(dimethylsiloxane) (PDMS) interface: Influence of pH and ionic strength on its conformation, adsorption, and aqueous lubrication properties. *Langmuir.* **2005**, *21*, 8344−8353.
(79) Symmes, B. A.; Stefanski, A. L.; Magin, C. M.; Evans, C. M. Role of mucins in lung homeostasis: regulated expression and biosynthesis in health and disease. *Biochem. Soc. Trans.* **2018**, *46*, 707−719.
(80) Cao, X.; Bansil, R.; Bhaskar, K. R.; Turner, B. S.; LaMont, J. T.; Niu, N.; Afdhal, N. H. pH-dependent conformational change of gastric mucin leads to sol-gel transition. *Biophys. J.* **1999**, *76*, 1250−1258.
(81) Tang, X.; Ostedgaard, L. S.; Hoegger, M. J.; Moninger, T. O.; Karp, P. H.; McMenimen, J. D.; Choudhury, B.; Varki, A.; Stoltz, D. A.; Welsh, M. J. Acidic pH increases airway surface liquid viscosity in cystic fibrosis. *J. Clin. Invest.* **2016**, *126*, 879−891.
(82) Wan, F.; Herzberg, M.; Huang, Z.; Hassenkam, T.; Nielsen, H. M. A free-floating mucin layer to investigate the effect of the local microenvironment in lungs on mucin-nanoparticle interactions. *Acta Biomater.* **2020**, *104*, 115−123.
(83) Zanin, M.; Baviskar, P.; Webster, R.; Webby, R. The Interaction between Respiratory Pathogens and Mucus. *Cell Host Microbe.* **2016**, *19*, 159−168.
(84) Yang, M.; Lai, S. K.; Yu, T.; Wang, Y.; Happe, C.; Zhong, W.; Zhang, M.; Anonuevo, A.; Fridley, C.; Hung, A.; Fu, J.; Hanes, J. Nanoparticle penetration of human cervicovaginal mucus: The effect of polyvinyl alcohol. *J. Controlled Release* **2014**, *192*, 202−208.
(85) Khutoryanskiy, V. V. Beyond PEGylation: Alternative surface-modification of nanoparticles with mucus-inert biomaterials. *Adv. Drug Delivery Rev.* **2018**, *124*, 140−149.
(86) Zhou, H.; Fan, Z.; Li, P.; Deng, J.; Arhontoulis, D. C.; Li, C.; Bowne, W. B.; Cheng, H. Dense and Dynamic Polyethylene Glycol Shells Cloak Nanoparticles from Uptake by Liver Endothelial Cells for Long Blood Circulation. *ACS Nano* **2018**, *12*, 10130−10141.
(87) Khalili, M.; Zhou, H.; Thadi, A.; Daniels, L.; Fan, Z.; Morano, W. F.; Ang, J.; Goldstein, E.; Polyak, B.; Mapow, B. C.; Cheng, H.; Bowne, W. B. Slippery Nanoparticles as a Diffusion Platform for Mucin Producing Gastrointestinal Tumors. *Ann. Surg. Oncol.* **2020**, *27*, 76−84.
(88) Lai, S. K.; Suk, J.; Pace, A.; Wang, Y.; Yang, M.; Mert, O.; Chen, J.; Kim, J.; Hanes, J. Drug carrier nanoparticles that penetrate human chronic rhinosinusitis mucus. *Biomaterials.* **2011**, *32*, 6285−6290.
(89) Keegan, M. E.; Falcone, J. L.; Leung, T. C.; Saltzman, W. M. Biodegradable microspheres with enhanced capacity for covalently bound surface ligands. *Macromolecules.* **2004**, *37*, 9779−9784.
(90) Bao, C.; Liu, B.; Li, B.; Chai, J.; Li, Y. Enhanced Transport of Shape and Rigidity-Tuned α-Lactalbumin Nanotubes across Intestinal Mucus and Cellular Barriers. *Nano Lett.* **2020**, *20*, 1352−1361.
(91) Pai, R. V.; Monpara, J. D.; Vavia, P. R. Exploring molecular dynamics simulation to predict binding with ocular mucin: An in silico approach for screening mucoadhesive materials for ocular retentive delivery systems. *J. Controlled Release* **2019**, *309*, 190−202.
(92) Prozeller, D.; Morsbach, S.; Landfester, K. Isothermal titration calorimetry as a complementary method for investigating nanoparticle-protein interactions. *Nanoscale.* **2019**, *11*, 19265−19273.
(93) De, M.; You, C. C.; Srivastava, S.; Rotello, V. M. Biomimetic interactions of proteins with functionalized nanoparticles: A thermodynamic study. *J. Am. Chem. Soc.* **2007**, *129*, 10747−10753.
(94) Shimokhina, N.; Bronowska, A.; Homans, S. W. Contribution of Ligand Desolvation to Binding Thermodynamics in a Ligand-Protein Interaction. *Angew. Chem., Int. Ed.* **2006**, *45*, 6231−6231.
(95) Hsein, H.; Garrait, G.; Beyssac, E.; Hoffart, V. Whey protein mucoadhesive properties for oral drug delivery: Mucin-whey protein interaction and mucoadhesive bond strength. *Colloids Surf., B* **2015**, *136*, 799−808.
(96) Cheng, Z.; Chen, X.; Zhai, D.; Gao, F.; Guo, T.; Li, W.; Hao, S.; Ji, J.; Wang, B. Development of keratin nanoparticles for controlled gastric mucoadhesion and drug release. *J. Nanobiotechnol.* **2018**, *16*, 24.
(97) Verma, A.; Stellacci, F. Effect of Surface Properties on Nanoparticle-Cell Interactions. *Small.* **2010**, *6*, 12−21.
(98) Gao, Y.; He, Y.; Zhang, H.; Zhang, Y.; Gao, T.; Wang, J.; Wang, S. Zwitterion-functionalized mesoporous silica nanoparticles for enhancing oral delivery of protein drugs by overcoming multiple gastrointestinal barriers. *J. Colloid Interface Sci.* **2021**, *582*, 364−375.
(99) Yaqub, N.; Wayne, G.; Birchall, M.; Song, W. Recent advances in human respiratory epithelium models for drug discovery. *Biotechnol. Adv.* **2022**, *54*, 107832.
(100) Nel, A.; Xia, T.; Madler, L.; Li, N. Toxic potential of materials at the nanolevel. *Science.* **2006**, *311*, 622−627.
(101) Cho, E. C.; Xie, J.; Wurm, P. A.; Xia, Y. Understanding the Role of Surface Charges in Cellular Adsorption versus Internalization by Selectively Removing Gold Nanoparticles on the Cell Surface with a I-2/KI Etchant. *Nano Lett.* **2009**, *9*, 1080−1084.
(102) Liu, M.; Wu, L.; Zhu, X.; Shan, W.; Li, L.; Cui, Y.; Huang, Y. Core-shell stability of nanoparticles plays an important role for overcoming the intestinal mucus and epithelium barrier. *J. Mater. Chem. B* **2016**, *4*, 5831−5841.

https://doi.org/10.1021/acsnano.2c11147
ACS Nano 2023, 17, 2813−2828

(103) Wu, J.; Zheng, Y.; Liu, M.; Shan, W.; Zhang, Z.; Huang, Y. Biomimetic Viruslike and Charge Reversible Nanoparticles to Sequentially Overcome Mucus and Epithelial Barriers for Oral Insulin Delivery. *ACS Appl. Mater. Interfaces.* **2018**, *10*, 9916−9928.
(104) Du, Q.; Ge, D.; Mirshafiee, V.; Chen, C.; Li, M.; Xue, C.; Ma, X.; Sun, B. Assessment of Neurotoxicity Induced by Different-Sized Stber Silica: Induction of Pyroptosis in Microglia. *Nanoscale.* **2019**, *11*, 12965−12972.
(105) Lai, S. K.; Wang, Y.; Wirtz, D.; Hanes, J. Micro- and macrorheology of mucus. *Adv. Drug Delivery Rev.* **2009**, *61*, 86−100.
(106) Crocker, J. C.; Grier, D. G. Methods of digital video microscopy for colloidal studies. *J. Colloid Interface Sci.* **1996**, *179*, 298−310.
(107) Lee, H.; Jeong, S. W.; Jung, E.; Lee, D. Dexamethasone-loaded H2O2-activatable anti-inflammatory nanoparticles for on-demand therapy of inflammatory respiratory diseases. *Nanomedicine.* **2020**, *30*, 102301.
(108) Nuutila, J.; Lilius, E. M. Flow cytometric quantitative determination of ingestion by phagocytes needs the distinguishing of overlapping populations of binding and ingesting cells. *Cytometry, Part A* **2005**, *65A*, 93−102.

https://doi.org/10.1021/acsnano.2c11147
ACS Nano 2023, 17, 2813−2828